Research Paper

GEOSPHERE

GEOSPHERE, v. 20, no. 5

https://doi.org/10.1130/GES02749.1

18 figures; 4 tables; 1 set of supplemental files

CORRESPONDENCE: farmer@colorado.edu

CITATION: Farmer, G.L., Morgan, L., Cosca, M., Mize, J., Bailley, T., Turner, K., Mercer, C., Ellison, E., and Bell, A., 2024, Mantle melting in regions of thick continental lithosphere: Examples from Late Cretaceous and younger volcanic rocks, Southern Rocky Mountains, Colorado (USA): Geosphere, v. 20, no. 5, p. 1411–1440, https://doi.org/10.1130/GES02749.1.

Science Editor: Christopher J. Spencer
Associate Editor: Eric H. Christiansen

Received 3 January 2024
Revision received 24 May 2024
Accepted 1 August 2024

Published online 9 September 2024

Mantle melting in regions of thick continental lithosphere: Examples from Late Cretaceous and younger volcanic rocks, Southern Rocky Mountains, Colorado (USA)

G. Lang Farmer[1], Leah Morgan[2], Michael Cosca[2], James Mize[1], Treasure Bailley[3], Kenzie Turner[2], Cameron Mercer[2], Eric Ellison[4], and Aaron Bell[4]

[1]Department of Geological Sciences and Cooperative Institute for Research in Environmental Sciences (CIRES), University of Colorado, Boulder, Colorado 80309, USA
[2]U.S. Geological Survey, Denver Federal Center, Denver, Colorado 80215, USA
[3]U.S. Environmental Protection Agency (EPA), Denver, Colorado 80202, USA
[4]Department of Geological Sciences, University of Colorado, Boulder, Colorado 80309, USA

ABSTRACT

Major- and trace-element data together with Nd and Sr isotopic compositions and $^{40}Ar/^{39}Ar$ age determinations were obtained for Late Cretaceous and younger volcanic rocks from north-central Colorado, USA, in the Southern Rocky Mountains to assess the sources of mantle-derived melts in a region underlain by thick (≥150 km) continental lithosphere. Trachybasalt to trachyandesite lava flows and volcanic cobbles of the Upper Cretaceous Windy Gap Volcanic Member of the Middle Park Formation have low $\varepsilon_{Nd}(t)$ values from −3.4 to −13, $^{87}Sr/^{86}Sr(t)$ from ~0.705 to ~0.707, high large ion lithophile element/high field strength element ratios, and low Ta/Th (≤0.2) values. These characteristics are consistent with the production of mafic melts during the Late Cretaceous to early Cenozoic Laramide orogeny through flux melting of asthenosphere above shallowly subducting and dehydrating oceanic lithosphere of the Farallon plate, followed by the interaction of these melts with preexisting, low $\varepsilon_{Nd}(t)$, continental lithospheric mantle during ascent. This scenario requires that asthenospheric melting occurred beneath continental lithosphere as thick as 200 km, in accordance with mantle xenoliths entrained in localized Devonian-age kimberlites. Such depths are consistent with the abundances of heavy rare earth elements (Yb, Sc) in the Laramide volcanic rocks, which require parental melts derived from garnet-bearing mantle source rocks. New $^{40}Ar/^{39}Ar$ ages from the Rabbit Ears and Elkhead Mountains volcanic fields confirm that mafic magmatism was reestablished in this region ca. 28 Ma after a hiatus of over 30 m.y. and that the locus of volcanism migrated to the west through time. These rocks have $\varepsilon_{Nd}(t)$ and $^{87}Sr/^{86}Sr(t)$ values equivalent to their older counterparts (−3.5 to −13 and 0.7038–0.7060, respectively), but they have higher average chondrite-normalized La/Yb values (~22 vs. ~10), and, for the Rabbit Ears volcanic field, higher and more variable Ta/Th values (0.29–0.43). The latter are general characteristics of all other post–40 Ma volcanic rocks in north-central Colorado for which literature data are available. Transitions from low to intermediate Ta/Th mafic volcanism occurred diachronously across southwest North America and are interpreted to have been a consequence of melting of continental lithospheric mantle previously metasomatized by aqueous fluids derived from the underthrusted Farallon plate. Melting occurred as remnants of the Farallon plate were removed and the continental lithospheric mantle was conductively heated by upwelling asthenosphere. A similar model can be applied to post–40 Ma magmatism in north-central Colorado, with periodic, east to west, removal of stranded remnants of the Farallon plate from the base of the continental lithospheric mantle accounting for the production, and western migration, of volcanism. The estimated depth of the lithosphere-asthenosphere boundary in north-central Colorado (~150 km) indicates that the lithosphere remains too thick to allow widespread melting of upwelling asthenosphere even after lithospheric thinning in the Cenozoic. The preservation of thick continental lithospheric mantle may account for the absence of oceanic-island basalt–like basaltic volcanism (high Ta/Th values of ~1 and $\varepsilon_{Nd}[t] > 0$), in contrast to areas of southwest North America that experienced larger-magnitude extension and lithosphere thinning, where oceanic-island basalt–like late Cenozoic basalts are common.

INTRODUCTION

Precambrian continental lithosphere, consisting of both ancient continental crust and underlying continental lithospheric mantle, is generally long-lived and thick, extending to depths as great as 300 km in some locations (Artemieva and Mooney, 2001; Carlson et al., 2005). At such lithospheric thicknesses, decompression melting of underlying asthenosphere is inhibited even if damp conditions (i.e., water undersaturated) or elevated (>1400 °C) potential temperatures might develop under thick continental lithosphere (McKenzie and Bickle, 1988; Lee et al., 2009; Niu, 2021). Nevertheless, well-documented examples exist of mantle melting in continental regions underlain by Precambrian

Lang Farmer https://orcid.org/0000-0003-1745-2305

lithosphere, as evidenced by Phanerozoic basaltic volcanism in the North China craton, Tibet, and southwestern North America (Farmer, 2022; Wu et al., 2019; Xia et al., 2011). In these areas, the development of continent-fringing convergent plate boundaries may have led to partial melting of both continental mantle lithosphere and upwelling asthenosphere through a complex interplay between changes in the composition of continental lithospheric mantle via infiltrating fluids or melts combined with the physical degradation and thinning of the preexisting mantle lithosphere (Menzies et al., 2007). Models of the apparent degradation of the continental lithospheric mantle, however, are based on proxy records provided by the ages and compositions of contemporaneous basaltic volcanic rocks and are limited by how well a given basalt can be attributed to melting of a specific mantle source in either the continental lithospheric mantle or underlying asthenosphere.

Some of the uncertainty in interpreting continental basalt proxy records could be allayed if the premagmatic structure and composition of the continental lithospheric mantle in a given location were better characterized, which would allow possible sources of the basalts to be better defined and help to establish the processes that would be required to induce upper-mantle melting. Such information is rarely available, but one exception is in the interior of southwestern North America, in the Southern Rocky Mountain region of north-central Colorado, USA. This region is underlain by Paleoproterozoic continental lithosphere that has been periodically affected by basaltic volcanism since the Late Cretaceous (Figs. 1–3). Unlike other regions worldwide, aspects of the physical and chemical composition of the continental lithospheric mantle and lower continental crust prior to the onset of magmatism can be reconstructed from mantle and crustal xenoliths entrained in Devonian-age kimberlites (the State Line kimberlite diatremes; Fig. 2), which demonstrate that the continental lithospheric mantle extended to depths of 200 km or more at that time (Eggler et al., 1987).

In this study, we combined information on the premagmatic continental lithospheric mantle with new and existing age and chemical data from Late Cretaceous and younger mafic to intermediate volcanic rocks in north-central

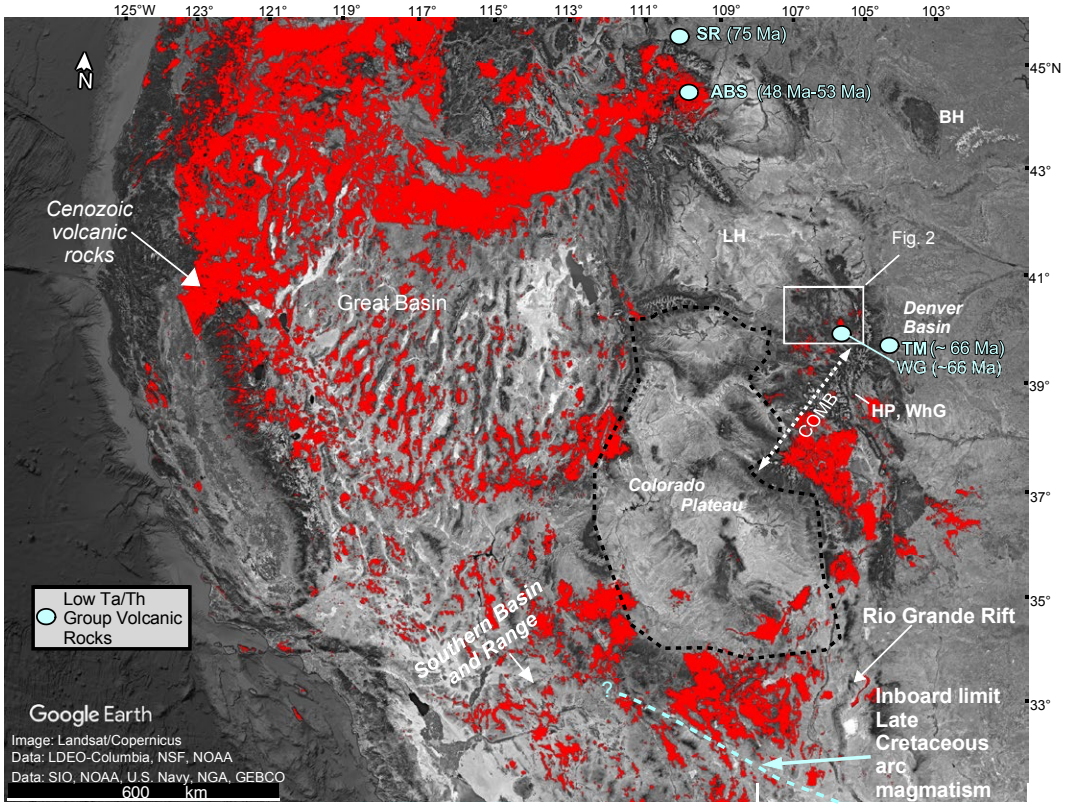

Figure 1. Distribution of Cenozoic volcanic rocks (red) in the western United States (from digital geologic maps of the U.S. states; https://mrdata.usgs.gov/geology/state/). SR—Sliderock Mountain volcanic field; ABS—Absaroka volcanic field; TM—Table Mountain; LH—Leucite Hills; BH—Black Hills; HP—Herring Park; WhG—Whitehorn Granodiorite; WG—Windy Gap. Range of Late Cretaceous to Cenozoic volcanic rock eruptive ages for select locations at eastern limit of volcanism is from du Bray and Harlan (1998), Feeley and Cosca (2003), Feeley et al. (2002), and Millikin et al. (2018). Eastern and northern limits of widespread Late Cretaceous volcanism in easternmost southern Basin and Range are based on data presented in Amato et al. (2017). Outlined box is study area in north-central Colorado, USA (Fig. 2). Dashed white line shows orientation and extent of Colorado Mineral Belt (COMB; after Burack-Wilson and Sims, 2003). Sources of imagery are: U.S. Navy, Lamont-Doherty Earth Observatory at Columbia University (LDEO-Columbia), National Science Foundation (NSF), National Oceanic and Atmospheric Administration (NOAA), Scripps Institution of Oceanography (SIO), National Geospatial-Intelligence Agency (NGA), General Bathymetric Chart of the Oceans (GEBCO).

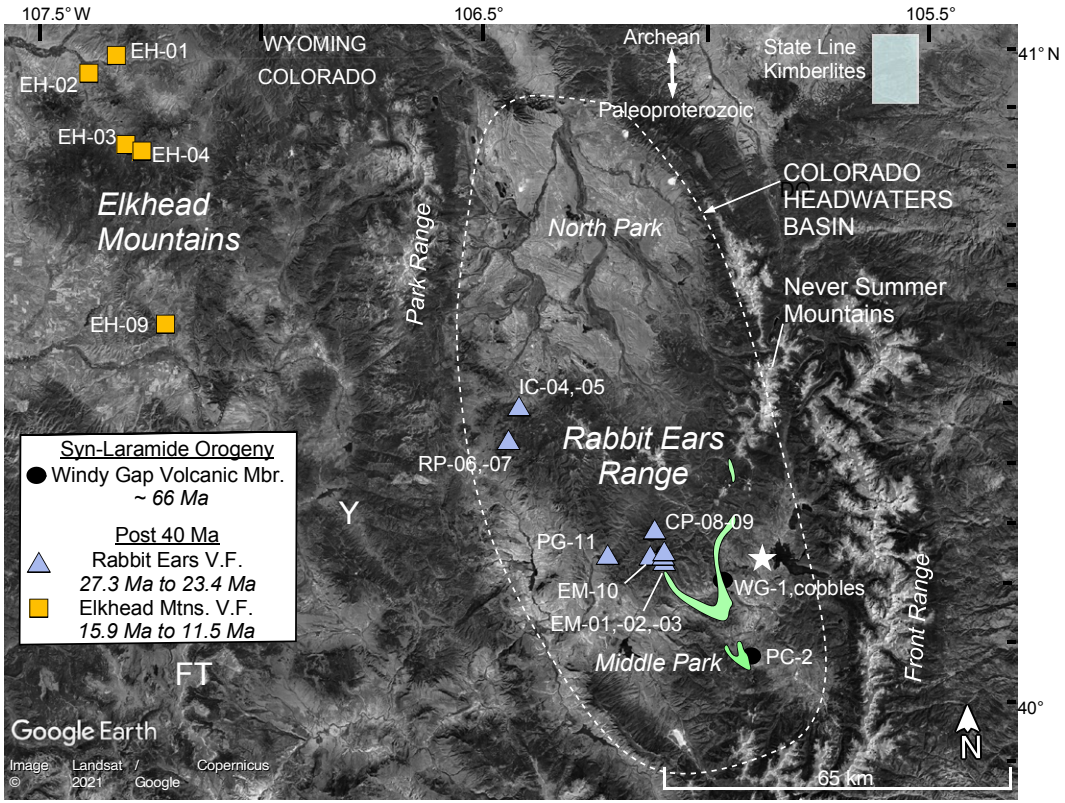

Figure 2. Volcanic rock sample locations and selected geologic features in north-central Colorado, USA. Sample locations are shown with symbols and labeled with abbreviated sample numbers from Table 1. Outline of syn-Laramide orogeny Colorado Headwaters Basin is from Cole et al. (2010). Y—Yampa; FT—Flat Tops; EM—Elk Mountain; PG—Pete's Gulch; CP—Corral Peak; RP—Ryder Peak; IC—Ironclad Mountain; V.F.—volcanic field. Outcrop area of Windy Gap (WG) Volcanic Member within the Breccia Spoon syncline is shown in light green. White star marks the location of 33 Ma olivine lamproite intrusive rock (Thompson et al., 1997).

Colorado to refine models for the physical and chemical evolution of the deep continental lithosphere in this region. Our study confirms that mantle melting beneath north-central Colorado led to both the pre–40 Ma, syncompressional volcanism synchronous with the Late Cretaceous to early Cenozoic Laramide orogeny and to younger, post–40 Ma, synextensional volcanism. Mafic volcanic rocks associated with both episodes have low $\varepsilon_{Nd}(t)$ values (<0) indicative of involvement of Precambrian continental lithospheric mantle in their generation, but the older volcanic rocks have low Ta/Th values compared to the higher (>0.2) and more variable Ta/Th values characteristic of the younger rocks. As proposed for Cenozoic volcanic rocks elsewhere in southwestern North America, the earlier episode was likely subduction-related magmatism initiated by flux-melting of asthenospheric mantle, albeit in the garnet peridotite stability field, while the younger episode reflects in situ melting of metasomatized continental lithospheric mantle triggered by heating induced by the removal of underthrusted oceanic lithosphere (Farmer et al., 2020). Unlike the Basin and Range Province in southwestern North America, the intermediate Ta/Th group volcanism in north-central Colorado has not yet been supplanted by basaltic magmatism related to decompression melting of upwelling asthenospheric mantle, likely as a consequence of the persistent thick mantle lithosphere known to have been present here since at least the late Paleozoic. Intermediate Ta/Th group mafic volcanic rocks in the Rabbit Ears volcanic field also carry disaggregated wehrlitized uppermost mantle material that is interpreted as evidence that metasomatism by silica-undersaturated carbonated melts was an early-stage process that preceded extension of the thick continental lithosphere in this region.

GEOLOGIC SETTING AND PREVIOUS WORK

The Southern Rocky Mountain region of north-central Colorado is underlain by Paleoproterozoic (1.78 Ga to 1.4 Ga) continental lithosphere that directly abuts the Archean Wyoming Province to the north (Fig. 2; Hill and Bickford,

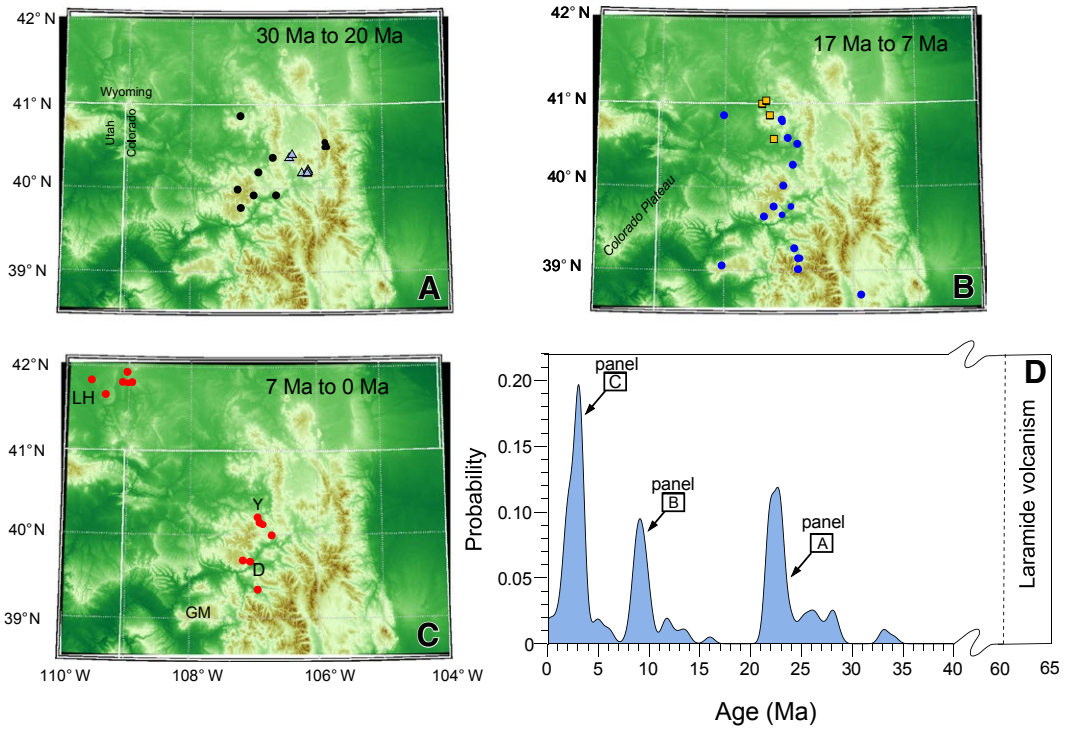

Figure 3. Space-time patterns for <65 wt% SiO_2, post–30 Ma volcanism in north-central Colorado, USA: (A) 30–20 Ma, (B) 17–7 Ma, (C) 7–0 Ma. LH—Leucite Hills; D—Dotsero; Y—Yampa; GM—Grand Mesa. (D) Relative probability plot for all 30 Ma and younger volcanic rocks (letters refer to panels A–C). Data are from this study (plotted with symbols from Fig. 2) and from multiple sources compiled by Farmer et al. (2020; filled circles).

2001; Morozova et al., 2005). During much of the Paleozoic and Mesozoic, the region lay at or below sea level and was periodically inundated by an epicontinental sea, as evidenced by the widespread occurrence of Paleozoic and Mesozoic marine sedimentary rocks in the region (Dickinson, 2004). Compressional tectonism and the development of basement-cored block uplifts accompanied the Laramide orogeny in the Late Cretaceous to early Cenozoic, followed by lithospheric extension beginning ca. 30 Ma, resulting in an increase in surface elevation to the present-day average of ~2 km (Tweto, 1975; Erslev, 1993; Landman and Flowers, 2013).

Phanerozoic igneous activity in north-central Colorado commenced in the Late Cretaceous, roughly synchronous with the Laramide orogeny. This igneous activity (hereafter referred to as Laramide magmatism) was the first to affect the region since the Mesoproterozoic, aside from the emplacement of the Devonian State Line kimberlites and a few silica-undersaturated, Cambrian intrusive igneous rocks found elsewhere in the Colorado (Fig. 2; Eggler et al., 1976; Lester et al., 2001; Hansen et al., 2013; Pivarunas and Meert, 2019). In general, the Laramide magmatism was confined spatially to the northeast-trending Colorado Mineral Belt (Fig. 1), as delineated today by a belt of alkalic to calc-alkalic intrusive igneous rocks (Mutschler et al., 1987). The latter are interpreted as the products of magmas produced in, or that had significant interaction with, lower continental crust (Stein and Crock, 1990). The goal of this study, however, was to assess the compositions of any mantle-derived melts present during igneous activity, information that is best extracted from the quenched magma compositions provided by volcanic rocks. In Colorado, preserved Laramide volcanic and volcaniclastic rocks are rare, but mafic- to intermediate-composition lavas flows and volcanic cobbles have been identified (Mutschler et al., 1987). The best characterized both chemically and isotopically are ca. 66 Ma trachybasaltic andesite to trachyandesite (i.e., shoshonite) lava flows from Table Mountain along the eastern flank of the Front Range (Figs. 1 and 2; Millikin et al., 2018; Musselman, 1987). However, mafic volcanic cobbles are also known from Late Cretaceous to Eocene volcaniclastic sedimentary rocks in north-central Colorado (Wilson, 2002). The only data available are major-element compositions of cobbles from the Windy Gap Volcanic Member of the Middle Park Formation in north-central Colorado (Figs. 1 and 2; Larson and Drexler, 1988), but these are significant because they demonstrate that trachybasalts are represented in the cobble population, which, in turn, is evidence that mantle melting likely occurred during the Laramide orogeny.

After a period of relative tectonic and igneous quiescence and establishment of the expansive Rocky Mountain erosional surface (Evanoff, 1990), renewed volcanic activity began in Colorado ca. 40 Ma (Cole et al., 2010; Kellogg, 1999; Tweto, 1979). This magmatism was no longer confined geographically to the Colorado Mineral Belt, but it was more generally aligned with the northward extension of the Rio Grande rift into Colorado (Fig. 1; Rosera et al., 2024). In central and southern Colorado, post–40 Ma volcanism was dominated by the large-volume, mid-Cenozoic (40–20 Ma) ignimbrite flareup that formed the Southern Colorado volcanic field (Lipman, 2007), followed by younger, synextensional, bimodal magmatism (Mutschler et al., 1987). The ignimbrite flareup did not extend to north-central Colorado, but synextensional mafic- to silicic-composition volcanic rocks younger than 40 Ma are common in this region and have been subject to extensive petrologic and geochemical study (Cosca et al., 2014; Gibson et al., 1991; Larson et al., 1975; Leat et al., 1988b, 1989, 1990, 1991; Thompson et al., 1990, 1993, 1997). The oldest and eastern-most volcanic rocks are the ca. 28 Ma trachybasalts to rhyolites of the Never Summer volcanic field (Braddock Peak volcanic field; Knox, 2005), whereas younger volcanism occurred periodically and increasingly farther to the west, from the Rabbit Ears volcanic field to the Elkhead, Flattops, and Yampa areas (Figs. 2 and 3). Volcanism is still active in the region near Dotsero (Fig. 3C), as demonstrated by the occurrence of postglacial trachybasalts (Rowe et al., 2011).

Establishing the sources and trigger mechanisms of mantle melting for both the Laramide and post–40 Ma magmatism is challenging, and little consensus exists on how and where mantle melting could have been initiated and sustained periodically over ~80 m.y. in essentially the same geographic location, far inboard of the plate boundary at the western margin of the continent (Larson and Drexler, 1988; Mutschler et al., 1987). For example, some workers have tied Laramide Colorado Mineral Belt magmatism to shallow subduction of oceanic lithosphere of the Farallon plate but recognized that a direct attribution to processes similar to those leading to arc magmatism is difficult because the Colorado Mineral Belt developed in a relatively narrow belt parallel rather than perpendicular to the relative motions of the North American and Farallon plates (Fig. 1; Chapin, 2012; Humphreys et al., 2003; Jones et al., 2011). Post–40 Ma mafic magmatism, in contrast, was largely synextensional and certainly related to partial mantle melting, but it remains unclear as to whether melting was initiated in the continental lithospheric mantle or underlying asthenosphere (Cosca et al., 2014; Eaton, 2008; Leat et al., 1988a; Mutschler et al., 1987).

The uncertainties regarding the origin of igneous activity in north-central Colorado stem in part from a poor understanding of the sources and trigger mechanism(s) of mantle melting during both the Laramide and post–40 Ma magmatic episodes. The unique aspect of north-central Colorado, compared to other inboard regions of southwestern North America and other areas of continental basaltic volcanism worldwide, is that aspects of the Phanerozoic structure and composition of the continental lithospheric mantle and deep continental crust prior to the onset of mafic magmatism can be inferred from mantle and crustal xenoliths entrained in the Devonian State Line kimberlites (Fig. 2). Petrologic and geochemical studies of these xenoliths have revealed that the Paleoproterozoic continental lithospheric mantle below the present-day Colorado-Wyoming (USA) border extended to depths of at least 200 km and was overlain by Paleoproterozoic continental crust that included ~15 km of mafic granulitic lower crust (Bradley and McCallum, 1984; Eggler et al., 1976, 1988; Carlson et al., 2004; Farmer et al., 2005). The continental lithospheric mantle consisted of infertile spinel and spinel/garnet peridotites at shallow levels separated from deeper-seated fertile garnet peridotites by a 10–15-km-thick swath of eclogite at depths of ~100 km (Eggler et al., 1988). Age information from Os, Hf, and Nd isotopic studies suggests that both fertile and infertile parts of the mantle lithosphere are Paleoproterozoic in age, similar in age to that of the overlying continental crust (Carlson et al., 2004). These data provide a reference frame in which to assess where and why mantle melting occurred beneath north-central Colorado.

STUDY AREA AND SAMPLES

A reassessment of the origin of magmatism in north-central Colorado requires a robust data set for mafic volcanic rocks from both magmatic episodes. Geochemical data for Laramide volcanic rocks are sparse in this area, so we obtained major- and trace-element data and whole-rock Nd and Sr isotopic analyses from mafic lava flows and mafic- to intermediate-composition volcanic cobbles from the Windy Gap Volcanic Member of the Middle Park Formation in north-central Colorado (Tables 1–4; Fig. 2). The Windy Gap Volcanic Member is a coarse, immature volcanic conglomerate deposited in the Laramide Colorado Headwaters Basin, with the latter roughly corresponding to the present-day North Park and Middle Park intermontane basins (Fig. 2; Cole et al., 2010; Dechesne et al., 2013). Similar Laramide-age volcaniclastic deposits are found farther to the southeast in the Denver Basin (Fig. 1), but these rocks have been more severely altered by groundwater interaction than those from the Windy Gap Volcanic Member (Larson and Drexler, 1988; Wilson, 2002). Volcanic cobbles in the Windy Gap Volcanic Member are mainly basalts to trachybasaltic andesites (Larson and Drexler, 1988; Taylor, 1975). Available $^{40}Ar/^{39}Ar$ ages indicate that the volcanic rocks found in this unit range in age from 65 Ma to 61 Ma and that the maximum depositional age for the conglomerates is ca. 60.5 Ma (Cole et al., 2010; Dechesne et al., 2013). Sedimentologic evidence suggests that the detritus was shed from a volcanic edifice located south of the Colorado Headwaters Basin (Fig. 2). The fact that the sedimentary deposits and interlayered basaltic lavas flows were deformed during the formation of the local Breccia Spoon syncline confirms that the volcanism was roughly synchronous with compressional tectonism related to the Laramide orogeny (Cole et al., 2010).

Two samples of mafic lava flows (04CO-PC-2, 04CO-WG-1) and seven mafic- to intermediate-composition volcanic cobbles (O4CO-WG-2A-H) were analyzed from the Windy Gap Volcanic Member at two locations along the east limb of the Breccia Spoon syncline (Table 1; Fig. 2; Taylor, 1975). These samples are

TABLE 1. SUMMARY OF CRETACEOUS AND YOUNGER VOLCANIC ROCKS, NORTH-CENTRAL COLORADO

Sample	Rock type*	Description†	Phenocryst assemblage§	Latitude# (DD N)	Longitude# (DD W)	Age** (Ma)	2σ
Elkhead Mountains volcanic field: Low Ta/Th group (?)							
13EH01	TBA	Dike, Sugarloaf Mtn.	Aphyric	41.0168	107.3211	12.7	± 0.1
13EH02	TA	Lava flow, Slater Creek Rd.	Aphyric	40.9826	107.3830	11.5	± 0.1
13EH03	TB	"	Aphyric	40.8530	107.2858	13.6	± 0.1
13EH04	TB	"	Aphyric	40.8489	107.2581	–	
13EH09	TBA	Lava flow, Hooker Mtn.	Aphyric	40.5560	107.2070	13.3	± 0.1
Rabbit Ears volcanic field: Intermediate Ta/Th group							
15-CO-EM-01	TBA	Lava flow, N. Elk Mtn.	Aphyric	40.1748	106.1279	26.4	± 0.1
15-CO-EM-02	TBA	Lava flow, N. Elk Mtn.	Aphyric	40.1769	106.1289	26.1	± 0.1
15-CO-EM-03	TBA	Lava flow, N. Elk Mtn.	Aphyric	40.1769	106.1310	26.2	± 0.1
16-CO-EM-10-WR	B	Dike, S. of Corral Peak	~25% megacrysts + glomerocrysts (ol > cpx)	40.1679	106.1474	25.4	± 1.4
16-CO-EM-10-NX	B	Dike, S. of Corral Peak	Matrix only (megacrysts removed by handpicking)	40.1679	106.1474	25.4	± 1.4
16-CO-IC-04	TB	Dike, Ironclad Mtn.	n.d.	40.4099	106.4449	25.7	± 0.1
16-CO-IC-05	TB	Dike, Ironclad Mtn.	~20% megacrysts + glomerocrysts (ol > cpx, tr bt/phl)	40.4094	106.4451	25.4	± 0.1
16-CO-RP-06	TB	Dike, Ryder Peak	~20% megacryst/glomerocrysts (ol > cpx)	40.3581	106.4570	25.2	± 0.1
16-CO-RP-07	TB	Dike, Ryder Peak	~20% megacryst/glomerocrysts (ol > cpx)	40.3595	106.4603	24.9	± 0.1
16-CO-CP-08	B	Lava flow, Corral Peak	Aphyric	40.2021	106.1521	23.4	± 0.2
16-CO-CP-09	B	Lava flow, Corral Peak	Aphyric	40.2030	106.1534	23.4	± 0.2
16-CO-PG-11	B	Lava flow, Pete's Gulch	Sparsely phyric, ~5% megacrysts-glomerocrysts (cpx)	40.1647	106.2494	27.3	± 0.4
Windy Gap Volcanic Member: Low Ta/Th groups							
04CO-WG-2A	TBA	Volcanic cobble	n.d.	40.1098	105.9999	66–60	–
04CO-WG-2B	TA	"	pl, cpx, tr hbl	40.1098	105.9999	"	–
04CO-WG-2C	TB	"	10%–20% ol > cpx	40.1098	105.9999	"	–
04CO-WG-2D	TBA	"	n.d.	40.1098	105.9999	"	–
04CO-WG-2E	TA	"	pl, cpx, tr hbl	40.1098	105.9999	"	–
04CO-WG-2G	TBA	"	n.d.	40.1098	105.9999	"	–
04CO-WG-2H	TA	"	n.d.	40.1098	105.9999	"	–
04CO-WG-1	TA	Lava flow	pl, cpx, tr hbl	40.1098	105.9999	"	–
04CO-PC-2	TA	"	pl, cpx, tr hbl	39.9798	105.9473	"	–

*Rock types are chemical classifications based on total alkali vs. SiO_2 (wt%) (total alkali–silica) values given in Table 2. TB—trachybasalt; TBA—trachybasaltic andesite; TA—trachyandesite; B—basalt.

†Mtn—Mountain; Rd—Road. " indicates same as previous cell.

§Phenocrysts refer to coarser grains (>1 mm). Mineral abbreviations: ol—olivine; cpx—clinopyroxene; tr—trace; bt/phl—biotite/phlogopite; pl—plagioclase; hbl—hornblende; n.d.—not determined.

#Sample locations given in decimal degrees (DD).

**Whole-rock ages from Supplemental Material Table S1 (see text footnote 1), except for age range for individual volcanic cobbles from the Windy Gap Volcanic Member of the Middle Park Formation, which is estimated from Ar-Ar ages reported by Cole et al. (2010).

composed of varying proportions of altered olivine (ol), feldspar (fsp), clinopyroxene (cpx), and biotite (bt) phenocrysts set in fine-grained matrices of fsp, opaque oxides, and altered glass (representative thin section images for these and other samples in study are available in Supplemental Material File S1[1]). A few partially altered amphibole (amp) grains were observed in samples 04CO-WG-2B and 04CO-WG-2H, but bt and amp phenocrysts were absent from the more mafic samples, and so they should be classified petrologically as basalts and not lamprophyres. We also included in our sample set three samples from Larson and Drexler (1988) (WG-4, WG-13, and WG-17) for which Nd and Sr isotopic analyses were performed.

In contrast, abundant age and major- and trace-element compositional data are available from basaltic rocks younger than 30 Ma in north-central Colorado, with the exceptions of ca. 26 Ma mafic volcanic rocks from the Rabbit Ears volcanic field and basaltic rocks from the younger (ca. 14 Ma) Elkhead

[1]Supplemental Material. Includes raw $^{40}Ar/^{39}Ar$ data and plots, electron microprobe mineral composition data, micro-Raman images and spectra, rock thin section images, and compilation of parameters used in petrogenetic models. Please visit https://doi.org/10.1130/GEOS.S.26506309 to access the supplemental material, and contact editing@geosociety.org with any questions.

TABLE 2. MAJOR-ELEMENT COMPOSITIONS (wt%) OF CRETACEOUS AND YOUNGER VOLCANIC ROCKS, NORTH-CENTRAL COLORADO

Sample	SiO_2	Al_2O_3	FeO^T	MnO	MgO	CaO	Na_2O	K_2O	TiO_2	P_2O_5	Total*	LOI	Mg#†
Elkhead Mountains volcanic field													
13EH01	53.6	14.9	8.62	0.12	6.94	7.18	3.42	3.20	1.48	0.51	98.7	1.26	59
13EH02	56.4	13.8	5.78	0.14	6.23	7.64	3.57	4.66	1.07	0.63	94.5	4.64	66
13EH03	49.5	14.2	10.6	0.16	9.59	8.11	3.63	1.98	1.67	0.53	95.8	4.61	62
13EH04	50.0	14.2	10.6	0.17	8.71	8.86	3.43	1.88	1.69	0.49	96.3	3.77	59
13EH09	54.8	14.8	7.77	0.12	7.03	6.44	4.53	2.52	1.43	0.47	95.8	4.31	62
Rabbit Ears volcanic field													
15-CO-EM-01	51.3	17.3	9.26	0.16	2.52	9.16	4.89	2.11	1.91	1.33	96.3	2.35	33
15-CO-EM-02	52.0	17.4	9.20	0.19	2.96	8.19	4.53	2.37	1.84	1.34	97.5	2.14	36
15-CO-EM-03	51.3	18.3	9.69	0.15	3.41	7.04	4.61	2.33	1.88	1.33	97.3	2.20	39
16-CO-EM-10-WR	45.4	13.2	10.2	0.15	11.7	11.6	3.37	1.19	2.54	0.70	98.0	1.37	67
16-CO-EM-10-NX	45.4	13.2	10.1	0.15	11.5	11.7	3.43	1.19	2.58	0.71	98.6	1.42	67
16-CO-IC-04	46.4	15.4	10.9	0.15	8.16	9.89	3.04	2.62	2.37	1.06	96.2	3.74	57
16-CO-IC-05	47.4	14.8	10.5	0.16	7.87	10.0	2.70	3.14	2.28	1.15	96.7	2.04	57
16-CO-RP-06	47.6	14.9	10.3	0.15	8.33	10.1	3.31	2.05	2.43	0.81	97.8	1.22	59
16-CO-RP-07	47.7	15.2	10.3	0.15	8.25	9.89	3.28	2.09	2.41	0.83	98.8	1.04	59
16-CO-CP-08	51.1	15.5	11.2	0.15	7.06	8.77	2.99	1.28	1.57	0.39	99.9	0.85	53
16-CO-CP-09	51.5	15.4	11.0	0.15	6.73	8.57	3.13	1.40	1.73	0.40	99.4	0.80	52
16-CO-PG-11	48.5	15.6	10.7	0.16	6.71	9.86	3.39	1.53	2.61	0.88	97.8	2.02	53
Windy Gap Volcanic Member, Middle Park Formation													
04CO-WG-2A	52.0	17.5	10.1	0.17	3.74	8.68	4.65	1.48	1.01	0.64	95.9	2.45	40
04CO-WG-2B	56.7	18.7	8.25	0.12	2.20	4.12	5.21	3.52	0.99	0.22	97.4	1.02	32
04CO-WG-2C	50.1	14.3	10.6	0.30	6.50	11.65	3.30	1.61	1.09	0.57	96.9	2.62	52
04CO-WG-2D	54.3	17.3	8.27	0.14	3.27	7.77	3.12	4.32	1.12	0.41	97.8	0.82	41
04CO-WG-2E	57.3	18.7	6.82	0.14	1.88	4.64	5.01	4.40	0.85	0.22	97.5	0.66	33
04CO-WG-2G	52.4	16.8	8.59	0.29	4.51	9.49	4.34	1.89	1.09	0.65	98.0	2.36	48
04CO-WG-2H	57.3	16.9	7.81	0.18	3.07	4.79	4.58	4.23	1.00	0.14	99.5	1.15	41
04CO-WG-1	55.5	17.4	8.56	0.19	2.83	5.80	4.00	4.14	1.08	0.50	95.6	3.61	37
04CO-PC-2	56.9	19.2	7.80	0.15	4.59	2.26	4.59	3.37	0.90	0.22	99.4	4.50	51

Notes: Whole-rock major-element abundances for Elkhead Mountains samples were determined by wavelength-dispersive X-ray fluorescence (WD-XRF) at SGS Minerals, Lakefield, Ontario, Canada. Major-element abundances of other samples were determined by inductively coupled plasma–mass spectrometry (ICP-MS) at Activation Laboratories, Ancaster, Ontario, Canada. All oxide percentages were renormalized to 100% (anhydrous). Actual analysis totals are reported in "Total" column. Total iron is reported as FeO^T.

*Reported totals, anhydrous (less loss on ignition [LOI]).

†Mg# calculated using FeO^T.

Mountains volcanic field farther to the west (Fig. 2). As a result, we focused our new investigations on these two areas.

Volcanic rocks of the ca. 26 Ma Rabbit Ears volcanic field are exposed in a northwest-oriented band that separates the North Park and Middle Park Basins (Fig. 2). Volcanic rocks here include basaltic- to silicic-composition lavas flows and pyroclastic rocks, some of which are crosscut by younger mafic-composition dikes. Basaltic- to intermediate-composition lavas and near-surface dike samples were obtained from several locations throughout the Rabbit Ears volcanic complex (Fig. 2). Whole-rock $^{40}Ar/^{39}Ar$ ages, major- and trace-element compositions, and Nd and Sr isotopic analyses were obtained from all of these rocks. Lava flows were sampled from Pete's Gulch at base of the volcanic section (PG-11), from higher in the section on the flanks of Elk Mountain (EM-01, EM-02, EM-03), and from the uppermost lava flows at Corral Peak (CP-08, CP-09) (Izett, 1966, 1968). The samples have distinctly different textures, with the Pete's Gulch sample containing ~3% ol and cpx megacrysts set in a matrix of finer-grained plagioclase (pl), cpx, and minor bt/phlogopite (phl). The Elk Mountain samples are aphyric, while the Corral Peak samples consist of ol and cpx megacrysts and smaller grains set in a medium-grained matrix dominated by randomly oriented pl laths and minor bt/phl. Bt/phl phenocrysts are absent from the lava flow samples, as is the case for the mafic dike samples apart from a few corroded grains found in one sample from Ironclad Mountain (16-CO-IC-04).

TABLE 3. TRACE-ELEMENT COMPOSITIONS (ppm) OF CRETACEOUS AND YOUNGER VOLCANIC ROCKS, NORTH-CENTRAL COLORADO

Sample	Sc	V	Cr	Co	Ni	Cu	Zn	Ga	Zr	Ba	Cs	Hf	Nb	Pb	Rb	Sb	Sr	Ta	Th	U	Y	La	Ce	Pr	Nd	Sm	Eu	Gd	Tb	Dy	Ho	Er	Tm	Yb	Lu	$(La/Yb)_N$	Ta/Th
Elkhead Mountains volcanic field																																					
13EH01	19	150	240	37	162	50	95	20	207	2940	0.6	6	13	19	38	<0.1	1530	0.60	4.3	1.9	19	47	96	12	43	7.3	2.1	5.3	0.74	3.9	0.71	1.9	0.26	1.5	0.22	21.1	0.14
13EH02	13	101	190	21	157	42	90	18	391	3410	0.2	11	15	26	47	<0.1	2430	<0.5	6.4	2.3	16	80	164	20	72	10	2.6	6.1	0.69	3.3	0.59	1.5	0.21	1.2	0.17	45.3	–
13EH03	23	189	330	45	180	56	103	18	140	1650	0.6	4	15	12	27	<0.1	1320	0.80	3.0	1.4	22	34	70	8.6	34	6.4	2.0	5.8	0.81	4.5	0.88	2.2	0.30	1.8	0.24	12.9	0.27
13EH04	24	191	300	45	178	55	99	19	137	1430	1.4	4	15	10	28	<0.1	1250	0.80	2.9	1.3	22	32	66	8.2	32	6.1	1.9	5.8	0.83	4.4	0.83	2.3	0.32	2.0	0.29	10.8	0.28
13EH09	16	158	250	44	143	40	88	21	164	1990	0.8	5	21	32	30	0.7	912	1.20	4.3	1.9	16	39	78	9.3	35	6.0	1.8	4.8	0.63	3.3	0.58	1.5	0.19	1.2	0.16	22.1	0.28
Rabbit Ears volcanic field																																					
15-CO-EM-01	9	131	<20	19	<20	10	120	21	180	1663	3.1	3.8	45	9	26	<0.2	1441	2.95	7.7	2.0	27	72	143	17	66	11	3.2	8.4	1.0	5.3	0.93	2.5	0.32	2.3	0.30	22	0.38
15-CO-EM-02	9	124	<20	20	<20	<10	120	21	223	1729	1	5.3	49	9	27	<0.2	1367	3.06	8.2	2.1	27	74	148	17	69	12	3.3	8.6	1.2	5.6	0.95	2.6	0.35	2.2	0.35	23	0.37
15-CO-EM-03	10	131	<20	19	<20	10	110	20	145	1798	1.7	3.3	46	9	35	<0.2	1329	2.98	7.8	2.0	26	72	144	17	68	12	3.2	8.5	1.1	5.4	0.94	2.6	0.33	2.2	0.31	22	0.38
16-CO-IC-04	24	248	240	41	100	60	100	18	280	2154	2.3	7.2	36	8	54	<0.2	1730	1.94	6.8	2.0	26	74	151	18	73	13	3.4	8.9	1.1	5.3	0.88	2.4	0.32	2.0	0.28	25	0.29
16-CO-IC-05	23	247	230	40	100	50	110	19	277	2240	0.8	7	36	9	63	0.4	1774	2.07	7.2	2.1	26	77	157	19	75	13	3.3	9.3	1.1	5.4	0.91	2.5	0.32	1.9	0.33	27	0.29
16-CO-RP-06	23	244	210	40	110	50	110	19	169	1633	1	4	32	5	31	0.3	1461	1.97	4.5	1.3	23	59	120	15	61	11	3.1	8.0	1.0	5.0	0.81	2.3	0.25	1.6	0.28	25	0.43
16-CO-RP-07	23	243	220	41	120	50	120	19	170	1529	0.6	4	33	5	34	<0.2	1446	1.99	4.3	1.2	23	57	118	14	59	11	3.0	7.8	1.0	4.9	0.82	2.1	0.27	1.6	0.26	24	0.46
16-CO-CP-08	22	188	220	42	110	40	130	19	120	484	0.5	3	12	<5	27	<0.2	572	0.75	2.4	0.6	22	25	55	6.8	29	6.2	1.9	5.8	0.84	4.4	0.81	2.2	0.31	2.0	0.29	8.6	0.32
16-CO-CP-09	23	199	210	43	120	40	120	20	125	508	0.3	3.3	13	<5	30	<0.2	523	0.77	2.6	0.7	24	25	55	6.8	29	6.5	1.9	6.0	0.87	4.8	0.86	2.4	0.34	2.1	0.30	8.2	0.30
16-CO-EM-10-WR	31	288	530	50	200	60	90	16	160	1617	0.7	3.8	35	5	24	<0.2	1396	2.12	6.4	1.6	22	70	140	17	66	12	3.3	8.1	0.96	4.8	0.77	2.1	0.27	1.6	0.22	30	0.33
16-CO-EM-10-NX	32	293	520	49	190	60	90	16	162	1653	0.8	3.9	35	<5	25	<0.2	1425	2.04	6.4	1.7	22	69	138	17	67	12	3.2	8.1	1.0	4.7	0.78	2.1	0.28	1.7	0.22	28	0.32
16-CO-PG-11	22	272	60	41	50.0	40	120	21	221	1531	0.6	5.3	37	7	22	0.4	1344	2.36	6.2	1.9	27	64	128	15	61	12	3.1	8.4	1.1	5.6	0.95	2.6	0.38	2.3	0.33	19	0.38
Windy Gap Volcanic Member, Middle Park Formation																																					
04CO-WG-2A	22	257	<20	27	30	100	140	22	146	994	2.9	3.9	19	12	9.0	<0.2	1094	1.2	6.3	2.1	25	36	72	7.8	31	6.2	1.9	5.1	0.81	4.4	0.82	2.37	0.35	2.2	0.35	11	0.19
04CO-WG-2B	17	207	<20	15	<20	20	100	19	200	1303	0.8	5.7	27	7	77	1.3	835	1.29	6.2	2.6	21	37	63	6.8	23	4.7	1.8	4.1	0.65	3.8	0.75	2.27	0.35	2.3	0.34	11	0.21
04CO-WG-2C	41	310	60	31	40	60	120	20	100	699	1.5	3	9.9	8	19	2.4	690	0.59	3.5	0.7	27	26	55	6.5	28	6.3	1.8	5.6	0.91	4.8	0.89	2.47	0.36	2.3	0.35	7.7	0.17
04CO-WG-2D	28	257	30	17	<20	30	130	21	124	967	0.2	3.7	13	12	79	3.8	887	0.70	3.0	0.9	20	22	45	5.4	21	4.8	1.8	4.2	0.67	3.7	0.7	2.1	0.32	2.0	0.29	7.6	0.23
04CO-WG-2E	16	135	20	13	<20	30	110	17	191	1156	0.8	4.9	15	<5	77	3.3	499	0.89	5.7	1.5	22	29	52	6.2	21	4.5	1.7	4.1	0.67	3.9	0.79	2.36	0.35	2.3	0.36	8.6	0.16
04CO-WG-2G	27	307	150	26	60	100	130	22	132	957	2.7	3.7	17	9	17	0.4	1022	1.03	5.2	1.0	25	33	68	7.5	31	6.2	1.8	5.4	0.85	4.5	0.83	2.39	0.35	2.2	0.34	10	0.20
04CO-WG-2H	17	195	30	20	20	40	120	16	349	1938	0.7	9.9	20	10	76	3.4	567	1.24	8.7	2.1	21	29	64	7.5	27	5.6	1.7	4.7	0.69	3.7	0.71	2.12	0.33	2.1	0.30	9.5	0.14
04CO-WG-1	20	245	<20	20	<20	40	130	21	142	1278	3	3.9	18	35	71	1.4	914	1.12	7.3	2.0	21	30	62	7.5	29	5.8	1.9	5.1	0.70	3.7	0.71	2.04	0.31	2.0	0.29	10	0.15
04CO-PC-2	20	162	<20	16	<20	20	100	24	182	1562	0.6	4.8	20	31	58	1.0	615	1.43	9.0	1.8	21	35	65	7.5	28	5.3	1.7	4.5	0.66	3.5	0.72	2.12	0.32	2.1	0.30	11	0.16
Reproducibility*	6	7	7	7	32	12	23	2	10	5	14	21	4	17	2	28	15	9	1	2	19	7	3	3	3	3	4	7	1	3	3	5	2	3	3		
Windy Gap Volcanic Member isotope-dilution concentrations†																																					
WG-4															20		873.0								46	7.8											
WG-13															32		1087								56	9.1											
WG-17															33		1257								50	8.0											

Notes: Whole-rock trace-element abundances (ppm) for Elkhead Mountains samples were determined by inductively coupled plasma–optical emission spectroscopy (ICP-OES) at SGS Minerals, Lakefield, Ontario, Canada. Other samples were determined by inductively coupled plasma–mass spectrometry (ICP-MS) at Activation Laboratories, Ancaster, Ontario, Canada, except where otherwise noted. See McDonough and Sun (1995) for $(La/Yb)_N$ normalization.

*Estimated external reproducibility is % of mean standard concentrations measured during study period for data obtained from Activation Laboratories.

†Isotope-dilution concentration determinations, performed at University of Colorado at Boulder. External reproducibilities were estimated at ~1% for Rb and Sr, and 0.5% for Sm and Nd. Samples are from Larson and Drexler (1988).

Mafic dike samples are from erosional remnants exposed in the northwest portions of the volcanic field at Ironclad Mountain and Ryder Peak (16-CO-IC-04, 16-CO-IC-05; 16-CO-RP-06, 16-CO-RP-07) and in the central part of the volcanic massif northwest of Elk Mountain (16-CO-EM-10; Fig. 2). These samples are texturally similar to the Pete's Gulch lava flow and consist of seriate porphyritic ol and cpx grains in a pl, cpx ± bt/phl matrix. Porphyritic grains are present in 5%–10% modal abundances in the Ironclad and Ryder Peak samples, but they constitute up to 25% of sample 16-CO-EM-10. The coarser crystals include ~2-cm-long individual ol and cpx megacrysts, as well as sparse cpx-ol glomerocrysts. The dike samples were subjected to electron microprobe analysis and micro-Raman imaging with the intent of determining the origin of the megacryst minerals.

TABLE 4. Sr AND Nd ISOTOPIC COMPOSITIONS OF CRETACEOUS AND YOUNGER VOLCANIC ROCKS, NORTH-CENTRAL COLORADO

Sample	$^{87}Rb/^{86}Sr$*	$^{87}Sr/^{86}Sr$†		$^{87}Sr/^{86}Sr(t)$§	$^{147}Sm/^{144}Nd$*	$^{143}Nd/^{144}Nd$#		$^{143}Nd/^{144}Nd(t)$§	$\varepsilon_{Nd}(t)$**
Elkhead Mountains volcanic field									
13EH01	0.072	0.704004	± 10	0.703994	0.1018	0.512185	± 11	0.512178	–8.72
13EH02	0.056	0.704079	± 12	0.704071	0.0867	0.511979	± 10	0.511973	–12.7
13EH03	0.059	0.704927	± 8	0.704919	0.1135	0.512312	± 7	0.512305	–6.25
13EH04	0.065	0.705977	± 9	0.705968	0.1168	0.512271	± 10	0.512263	–7.06
13EH09	0.095	0.703883	± 8	0.703870	0.1046	0.512266	± 45	0.512259	–7.14
Rabbit Ears volcanic field									
15-CO-EM-01	0.052	0.705186	± 8	0.705166	0.1028	0.512386	± 9	0.512368	–4.60
15-CO-EM-02	0.057	0.703927	± 11	0.703906	0.1043	0.51237	± 18	0.512349	–4.98
16-CO-EM-10-WR	0.050	0.704320	± 12	0.704303	0.1072	0.512443	± 63	0.512427	–3.52
16-CO-EM-10-NX	0.051	0.704347	± 16	0.704330	0.1053				
16-CO-IC-04	0.090	0.705017	± 19	0.704984	0.1105	0.512281	± 19	0.512264	–6.65
16-CO-IC-05	0.103	0.704811	± 14	0.704774	0.1097	0.512258	± 9	0.512241	–7.10
16-CO-RP-06	0.061	0.704319	± 12	0.704297	0.1298	0.512386	± 18	0.512368	–4.63
16-CO-RP-07	0.068	0.704396	± 37	0.704372	0.1350	0.512377	± 32	0.512360	–4.80
16-CO-CP-08	0.136	0.705990	± 13	0.705944	0.1068	n.d.			
16-CO-CP-09	0.166	0.706081	± 8	0.706025	0.1061	0.512339	± 24	0.512319	–5.62
16-CO-PG-11	0.047	0.704562	± 8	0.704544	0.1147	0.512379	± 19	0.512360	–4.74
Windy Gap Volcanic Member, Middle Park Formation									
04CO-WG-2A	0.004	0.704884	± 12	0.704862	0.1202	0.512328	± 13	0.512277	–5.39
04CO-WG-2B	0.003	0.706381	± 10	0.706133	0.1220	0.512008	± 14	0.511960	–11.6
04CO-WG-2C	0.008	0.705125	± 13	0.705049	0.1361	0.512292	± 23	0.512236	–6.19
04CO-WG-2D	0.004	0.705373	± 11	0.705149	0.1387	0.512273	± 20	0.512219	–6.52
04CO-WG-2E	0.009	0.706349	± 12	0.705938	0.1284	0.512074	± 14	0.512022	–10.4
04CO-WG-2G	0.005	0.704902	± 14	0.704858	0.1238	0.512328	± 13	0.512276	–5.41
04CO-WG-2H	0.006	0.707132	± 15	0.706788	0.1262	0.511936	± 12	0.511885	–13.0
04CO-WG-1	0.007	0.706154	± 14	0.705943	0.1198	0.512247	± 14	0.512197	–6.95
04CO-PC-2	0.007	0.707432	± 8	0.707183	0.1138	0.512041	± 15	0.511992	–10.9
WG-4††	0.065	0.705189	± 9	0.705132	0.1017	0.512262	± 15	0.512220	–6.58
WG-13††	0.086	0.705058	± 9	0.704982	0.0974	0.512337	± 14	0.512297	–5.08
WG-17††	0.071	0.705190	± 8	0.705123	0.0976	0.512424	± 11	0.512384	–3.38

Notes: Total procedural blanks averaged ~1 ng for Sr and 100 pg for Nd during the study period.
*Ratios calculated from inductively coupled plasma–mass spectrometry (ICP-MS) concentration determination listed in Table 2, except for WG samples, which are from isotope-dilution determinations presented in Table 3.
†Measured $^{87}Sr/^{86}Sr$ ratios were analyzed using four-collector static mode measurements. Errors are 2σ of mean and refer to last two digits of the $^{87}Sr/^{86}Sr$ ratio.
§Initial isotopic compositions calculated using ages given in Table 1, with the exception of Windy Gap WG samples, which were calculated at 62.5 Ma.
#Measured $^{143}Nd/^{144}Nd$ normalized to $^{146}Nd/^{144}Nd = 0.7219$. Samples were analyzed using dynamic mode three-collector measurements.
**ε_{Nd} values calculated using present-day $^{143}Nd/^{144}Nd(CHUR) = 0.512638$, where CHUR indicates calculation relative to chondritic uniform reservoir.
††Basalt cobbles from Larson and Drexler (1988).

The Miocene Elkhead Mountains volcanic field is located west of the Park Range, extending to the Wyoming border, and it includes a series of eroded volcanic centers, sills, and lava flows including bt-bearing minettes (Fig. 2; Leat et al., 1988b). Regional K-Ar ages indicate volcanism in the Elkhead Mountains occurred between 11.1 Ma and 7.6 Ma (Luedke and Smith, 1978). Sample 13EH01 is a basaltic dike intruding Miocene sediments at Sugarloaf Mountain with fresh ol phenocrysts in a fine-grained matrix of pl and iron oxides. Sample 13EH02 is an ol-bearing trachyandesite (minette) containing fresh bt set in a fine-grained groundmass of pl, cpx, and iron oxides. This sample was collected from an outcrop of columnar basalts along Slater Creek Road. Samples 13EH03 and 13EH04 are trachybasalts collected from a thick sequence of lava flows along Slater Creek Road. Both samples contain partially replaced ol (iddingsite) within a groundmass of pl, cpx, and iron oxides. Sample 13EH09 is trachybasaltic andesite collected from a thick (~20 m) lava flow on the west side of Hooker Mountain. This sample contains ol phenocrysts largely replaced with smaller cpx and bt phenocrysts in groundmass of pl and iron oxides.

ANALYTICAL TECHNIQUES

$^{40}Ar/^{39}Ar$ Age Determinations

Whole-rock fragments of volcanic rock ~1–1.7 mm in diameter were obtained by crushing, washing in deionized water, and handpicking for $^{40}Ar/^{39}Ar$ analysis. The washed samples were loaded into Al discs along with the neutron flux monitor Fish Canyon sanidine. Discs were wrapped in Al foil and sealed under vacuum in a quartz glass vial, which was wrapped in Cd foil. Two separate packages for the Elkhead and Rabbit Ears samples, respectively, were irradiated at the U.S. Geological Survey (USGS) TRIGA reactor.

Samples and standards were analyzed on a Thermo Scientific ARGUS VI mass spectrometer at the USGS Argon Geochronology Laboratory in Denver, Colorado. Gas release was accomplished by heating using a Photon Machines 50 W CO_2 laser. Noble gas purification was achieved with SAES getters and a cryogenic trap. Argon isotopes were detected using four Faraday detectors (^{40}Ar, ^{39}Ar, ^{38}Ar, and ^{37}Ar) and one ion counter (^{36}Ar), and measured abundances were determined using the MassSpec software package (authored by Al Deino, Berkeley Geochronology Center, Berkeley, California, USA). Background measurements were run every 3–5 analyses; argon isotopic backgrounds were determined by fitting data with a weighted mean ± 1σ. Discrimination and detector intercalibration factors were determined via measurements of three air pipettes approximately twice per day, using the atmospheric $^{40}Ar/^{36}Ar$ value of Lee et al. (2006). Samples were co-irradiated with Fish Canyon sanidine (FCs), and ages were calculated using an age for FCs of 28.201 ± 0.023 Ma (1σ) (Kuiper et al., 2008). Decay constants used were those of Min et al. (2000) for ^{40}K and Stoenner et al. (1965) for ^{37}Ar and ^{39}Ar. Nuclear interference production ratios for $(^{40}Ar/^{39}Ar)_K$, $(^{36}Ar/^{37}Ar)_{Ca}$, and $(^{39}Ar/^{37}Ar)_{Ca}$ were based on measurements of potassium-rich glass and CaF_2 co-irradiated with samples; values used were 0.0015105 ± 0.0006117, 0.0002673 ± 8.139000e–7, and 0.000754 ± 0.0000375, respectively. Other interferences were corrected using values for Cd-shielded fission-spectrum neutrons from Renne et al. (2005).

Whole-Rock Major-Element and Trace-Element Compositions and Nd and Sr Isotopic Analyses

Whole-rock major-element and trace-element determinations from the Elkhead Mountains volcanic field were obtained by wavelength-dispersive X-ray fluorescence spectroscopy (WD-XRF) and inductively coupled plasma–optical emission spectrometry (ICP-OES), respectively, at SGS Minerals, Lakefield, Ontario, Canada (Tables 2 and 3). Major- and trace-element data from Rabbit Ears volcanic field and Windy Gap Volcanic Member were obtained commercially by ICP-OES and ICP–mass spectrometry (ICP-MS), respectively, at Activation Laboratories, Ltd., Ancaster, Ontario (Tables 2 and 3).

Sr and Nd isotopic analyses were obtained from powdered whole-rock samples that were first dissolved in open containers in hydrofluoric and perchloric acids. Residues from the initial dissolutions were heated in hydrofluoric and nitric acids in sealed Teflon® containers until complete dissolution was achieved. Sr and rare earth elements (REEs) were then separated from the dissolved rock samples using Eichrom® Sr resin and Eichrom® TRU resin, respectively, using low-molarity nitric acid in ¼ inch (0.6 cm) inner diameter (ID) polytetrafluoroethylene (PTFE) columns (Pin et al., 1994). Nd was isolated from the REE concentrates using Eichrom® Ln resin in silica glass columns (3 mm ID, 14 cm long) with low-molarity hydrochloric acid (Pin et al., 1994). All isotopic analyses were completed at the Thermal Ionization Mass Spectrometry Laboratory at the University of Colorado, Boulder, Colorado, using an extensively refurbished Finnigan-MAT six collector solid source mass spectrometer (Table 4). Eight measurements of SRM-987 strontium isotopic standard during the study period yielded a mean value of $^{87}Sr/^{86}Sr$ = 0.71029 ± 2 (2σ mean). Seven measurements of the La Jolla Nd standard during the study period yielded a mean value of $^{143}Nd/^{144}Nd$ = 0.511835 ± 8 (2σ mean).

Electron Microprobe Mineral Analyses

Compositional data from ol megacrysts from Elk Mountain, Ryder Peak, and Ironclad Peak, and cpx megacrysts from Ryder Peak, at the Rabbit Ears volcanic field, were acquired with a JEOL 8230 electron microprobe housed in the Department of Geological Science at the University of Colorado at Boulder. The instrument is equipped with five tunable wavelength-dispersive spectrometers. Analyses were obtained using 15 keV accelerating potential, a 10 nA beam current, and a 2-µm-diameter beam. Peak counting times were 30 s, and off-peak counting times were 15 s. The off-peak correction utilized a linear background model for all elements. Standards consisted of suite of natural silicate minerals and oxides from Astimex, Inc. All data were dead-time corrected and reduced with a ZAF matrix correction algorithm that employed mass absorption coefficients sourced from the FFAST database (Chantler et al., 2005).

Micro-Raman Spectroscopy

Raman hyperspectral maps of petrographic thin sections from sample 16-CO-EM-10 from Elk Mountain, at the Rabbit Ears volcanic field, were obtained at the Raman Microspectroscopy Laboratory, Department of Geological Sciences, University of Colorado at Boulder, using a Horiba LabRam HR Evolution Raman spectrometer. A 532 nm laser was focused onto the sample surface, forming an ~2 µm spot with ~29 mW laser power. The sample was mapped with 2 µm step sizes and 1–3 s total acquisition time per pixel. Hyperspectral map data sets were background corrected using polynomial baseline subtraction. Mineralogy maps were generated using classical least squares fitting, with end-member spectra selected from within the data set by averaging areas containing homogeneous spectra. The end-member spectra were identified by matching the results with spectra in the RRUFF™ Project database (https://rruff.info; Lafuente et al., 2015).

RESULTS

$^{40}Ar/^{39}Ar$ Age Determinations

Whole-rock $^{40}Ar/^{39}Ar$ plateau and $^{39}Ar/^{40}Ar$ versus $^{36}Ar/^{40}Ar$ isochron ages for samples from the Elkhead Mountains and Rabbit Ears volcanic fields are summarized in Table 1, with more detailed analytical information available in Mercer et al. (2024) and in Supplemental Material File S2. Preferred ages generally correspond to analyses with mean square of weighted deviates (MSWD) values between 0.5 and 2.5. For most samples, the plateau and isochron ages are identical within analytical errors, except for sample PG-11 from the Rabbit Ears volcanic field, for which the plateau age was selected. Individual isochrons and release spectra for the Rabbit Ears samples are available in Supplemental Material File S3.

Ages of basalts and trachybasaltic andesites from the Rabbit Ears volcanic field range from 23.4 Ma to 27.3 Ma. The stratigraphically lowest sample from Pete's Gulch (PG-11) has the oldest age (27.3 ± 0.4 Ma), and lava from the stratigraphically highest level sampled, at Corral Peak (CP-08), has the youngest age (23.4 ± 0.3 Ma). The other lava samples (EM-01–03) from within volcanic succession have indistinguishable ages at an average value of ca. 26.2 Ma, which are also consistent with their position in the volcanic stratigraphy. Dike samples from Ironclad Mountain (16-CO-IC-04, 16-CO-IC05), Ryder Peak (16-CO-RP-06, 16-CO-RP-07), and from northwest of Elk Mountain (16-CO-EM-10) have similar ages ranging from 25.4 Ma to 25.5 Ma. Overall, these data indicate that the Rabbits Ears volcanic field was active for ~4 m.y. between 27 Ma and 23 Ma.

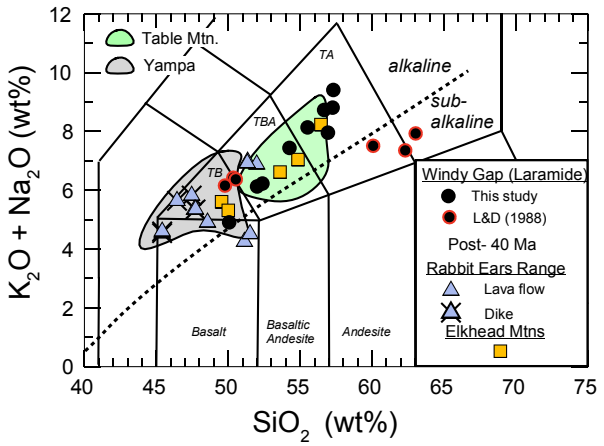

Figure 4. Whole-rock $K_2O + Na_2O$ vs. SiO_2 (wt%; total alkali–silica) diagram for samples analyzed in this study. Fields for mafic to intermediate compositions volcanic rocks from Table Mountain and Yampa from Cosca et al. (2014) and Millikin et al. (2018). Classification scheme is from Le Maitre (1989). TB—trachybasalt; TBA—trachybasaltic andesite; TA—trachyandesite. Dashed line separating alkaline from subalkaline volcanic rocks is from Irvine and Baragar (1971). L&D—Larson and Drexler (1988).

Mafic lavas from the Elkhead Mountains volcanic field have $^{40}Ar/^{39}Ar$ ages ranging from 13.6 Ma to 11.4 Ma. The sample with the oldest age (13EH03) has a $^{40}Ar/^{39}Ar$ plateau age of 13.61 ± 0.5 Ma, and the youngest sample (13EH02) has a $^{40}Ar/^{39}Ar$ plateau age of 11.44 ± 0.01 Ma. The Elkhead Mountain samples generally have similar $^{40}Ar/^{39}Ar$ plateau and $^{39}Ar/^{40}Ar$ versus $^{36}Ar/^{40}Ar$ isochron ages, except for sample 13EH04, which had trapped argon of nonatmospheric values and did not yield a $^{40}Ar/^{39}Ar$ plateau but yielded a $^{39}Ar/^{40}Ar$ versus $^{36}Ar/^{40}Ar$ isochron age of 15.7 ± 0.2 Ma.

Whole-Rock Major- and Trace-Element Compositions and Isotopic Compositions

Major-element compositions for the Rabbit Ears volcanic field samples are all alkalic and range from basalt and trachybasalt to trachybasaltic andesite (Table 2; Fig. 4). The most mafic rocks are the three dike samples (Mg# = 57–67; Table 2). Samples from the Windy Gap Volcanic Member and from the Elkhead Mountains volcanic field are also alkalic and range from trachybasalts to trachyandesites (Table 2; Fig. 4). Major-element abundances generally overlap for samples from all three localities, except that samples from the Rabbit Ears volcanic field have higher wt% TiO_2 (1.5% to 2.5%) and wt% P_2O_5 (0.4% to 1.3%) at any given wt% MgO (Fig. 5). Most of the Elkhead Mountains samples have wt% TiO_2 (~1.5%) intermediate between the Rabbit Ears volcanic field and Windy Gap Volcanic Member values.

All the analyzed rocks are enriched in light REEs (LREEs), although most samples from the Rabbit Ears and Elkhead Mountains volcanic fields have higher $(La/Yb)_N$ values (average ~22) than those from the Windy Gap Volcanic Member (average $[La/Yb]_N$ ~10) (Table 3; Figs. 6A–6C). All samples have similar heavy REE (HREE) abundances. The Windy Gap Volcanic Member and Elkhead Mountains volcanic field samples have overall trace-element abundances characterized by pronounced relative Nb and Ta depletions on a normalized trace-element plot and positive spikes in normalized Pb abundances (Figs. 7A–7B). The Rabbit Ears volcanic field samples, in contrast, have higher Nb and Ta abundances, consistent with their higher wt% TiO_2, and they lack prominent, positive normalized Pb abundance anomalies (Figs. 5 and 7C).

The most mafic samples (wt% MgO > ~7; Mg# = 52–67) from all three localities have similar $\varepsilon_{Nd}(t)$ values that range from –3.5 to –7.1 independent of eruptive age (Table 4; Figs. 8A and 9). The remaining samples also have Nd isotopic compositions in this range, except for several samples with wt% MgO <~6 from the Windy Gap Volcanic Member and Elkhead Mountains that have lower $\varepsilon_{Nd}(t)$ values from –10.4 to –13 (Fig. 8A). Initial $^{87}Sr/^{86}Sr$ values for samples from both the Rabbit Ears and Elkhead Mountains volcanic fields vary from ~0.7039 to ~0.7060, independent of the bulk or Nd isotopic compositions. Initial $^{87}Sr/^{86}Sr$ values for the Windy Gap Volcanic Member samples

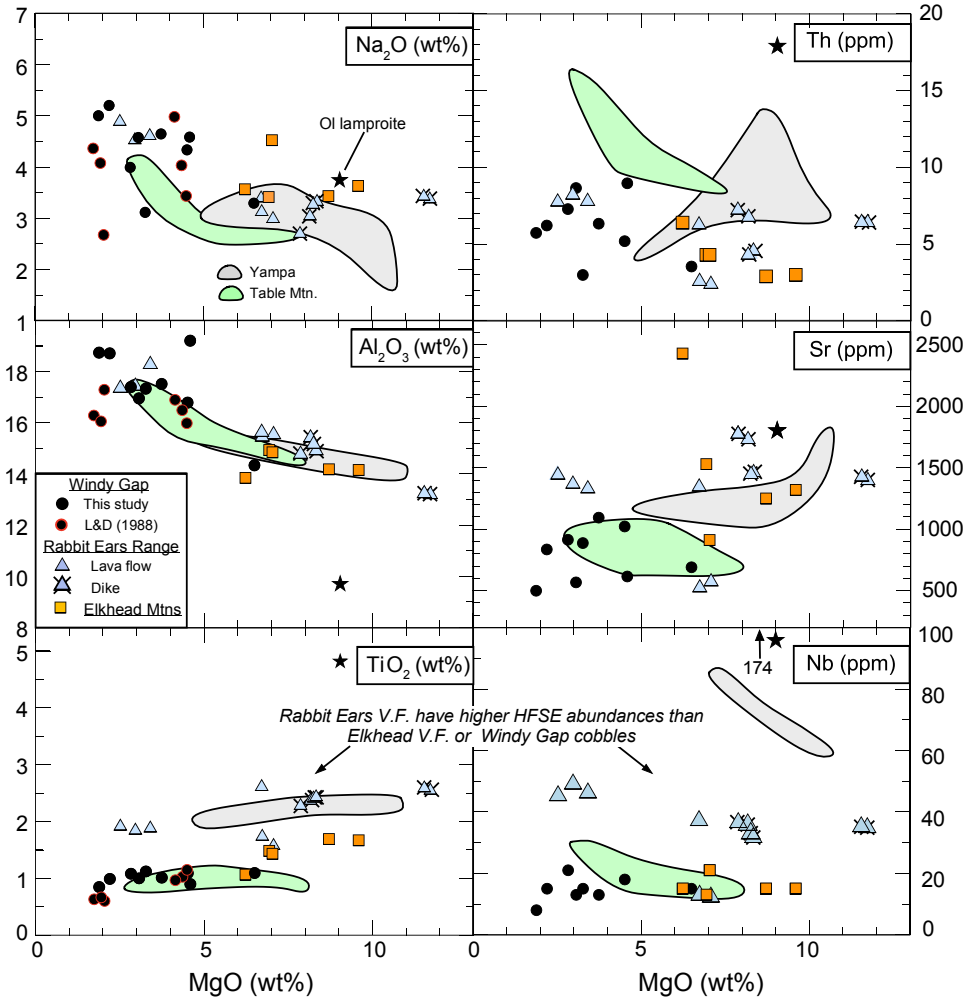

Figure 5. Select major- and trace-element abundances vs. MgO (wt%). L&D—Larson and Drexler (1988); Ol—olivine; V.F.—volcanic field; HFSE—high field strength elements.

are also variable but range to values as high as 0.7072 for the lower wt% MgO samples (Figs. 8B and 9).

Dike Sample Micro-Raman Petrography and Mineral Chemistry

Olivine megacrysts from the Elk Mountain dike (sample 06CO-EM-10) have Mg# ranging from 89 to 76 with Ca contents that range from 1200 ppm to 1500 ppm (Fig. 10A). Megacryst rims and smaller ol phenocrysts have lower Mg# (78–75) and range to higher Ca contents, ranging from 1500 ppm to 2600 ppm, which increase with decreasing Mg#. Olivine megacrysts from Ryder Peak and Ironclad Mountain localities fall on these same compositional trends, but the Ryder Peak grains with the lowest Ca content (1300 ppm) have forsterite contents from 80% to 82% ($Fo_{80–82}$), and Ironclad Mountain samples have Fo_{77} (Supplemental Material File S4). Clinopyroxene megacrysts from the Ryder Peak dike samples are low Cr (<0.5 wt% Cr_2O_3) diopsides (Fig. 10B). Rims on the diopside grains generally have higher wollastonite (Wo) components, lower wt% CaO and wt% Al_2O_3, and higher wt% FeO than their cores (Figs. 10B and 10C).

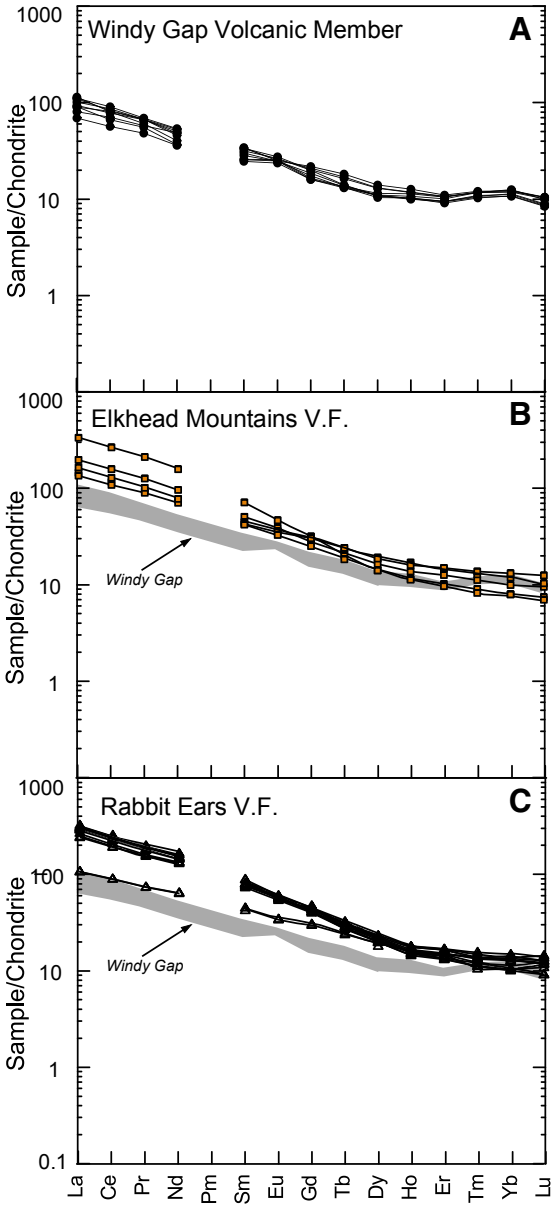

Figure 6. Chondrite-normalized rare earth element patterns for volcanic rocks from: (A) Windy Gap volcanic member, (B) Elkhead Mountains volcanic field (V.F.), and (C) Rabbit Ears volcanic field. Normalization values are from McDonough and Sun (1995).

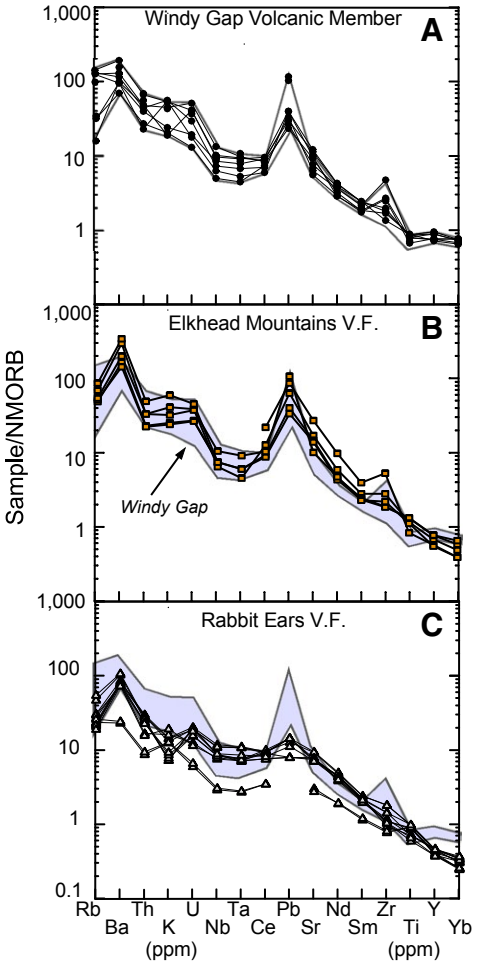

Figure 7. Normal mid-ocean ridge basalt (NMORB)–normalized trace-element abundances for volcanic rocks from: (A) Windy Gap volcanic member, (B) Elkhead Mountains volcanic field (V.F.), and (C) Rabbit Ears volcanic field. Normalization values are from Sun and McDonough (1989) and McCulloch and Gamble (1991).

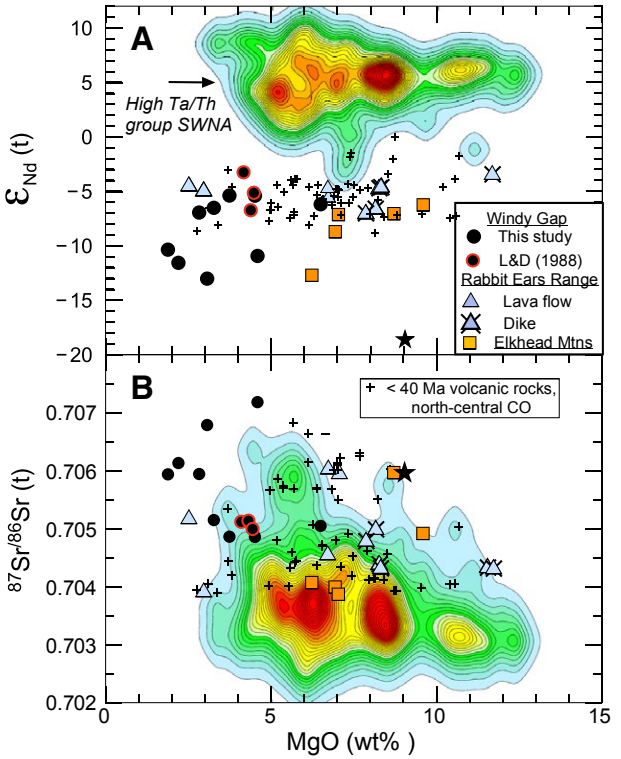

Figure 8. (A–B) Whole-rock neodymium (A) and strontium (B) isotopic compositions vs. MgO (wt%). Data from olivine lamproite (Thompson et al., 1997) are shown as a star. Data from <65% SiO_2, Cenozoic high Ta/Th volcanic rocks from southwestern North America (SWNA; shown as a smoothed two-dimensional histogram following Eilers and Goeman, 2004) and post–40 Ma volcanic rocks in north-central Colorado (CO), USA (crosses) from data set compiled in Farmer et al. (2020) are shown for comparison. L&D—Larson and Drexler (1988).

Ol and cpx megacrysts from Elk Mountain commonly contain ovoid, former melt pockets up to 400 µm in diameter, which we refer to as melts pockets for simplicity (Figs. 11A and 11C). Micro-Raman analysis of an ol-hosted melt pocket indicates that it contains abundant analcime (anl), but the pocket margins are also dominated by nepheline (nph) and fsp (Fig. 11B; Supplemental Material Fig. S1). The melt pocket imaged from a cpx-hosted megacryst contains varying proportions of 50–100-µm-sized nph, fsp, and ol, along with accessory apatite (ap), titanite (ttn), bt/phl, and opaque minerals (Fig. 11D; Supplemental Material Fig. S1). Micro-Raman analysis of the host basalt shows that its groundmass contains no nph and little ol (<1%) and is instead dominated by cpx (~40%), followed in modal abundance by fsp (19%), anl (17.7%), ap (9%), opaques (7.5%), and bt/phl (4.5%) (Supplemental Material Fig. S2).

DISCUSSION

Our new data demonstrate that the trachybasalt to trachyandesite volcanic cobbles in the Laramide Windy Gap Volcanic Member have low $\varepsilon_{Nd}(t)$ values (<–3.4)

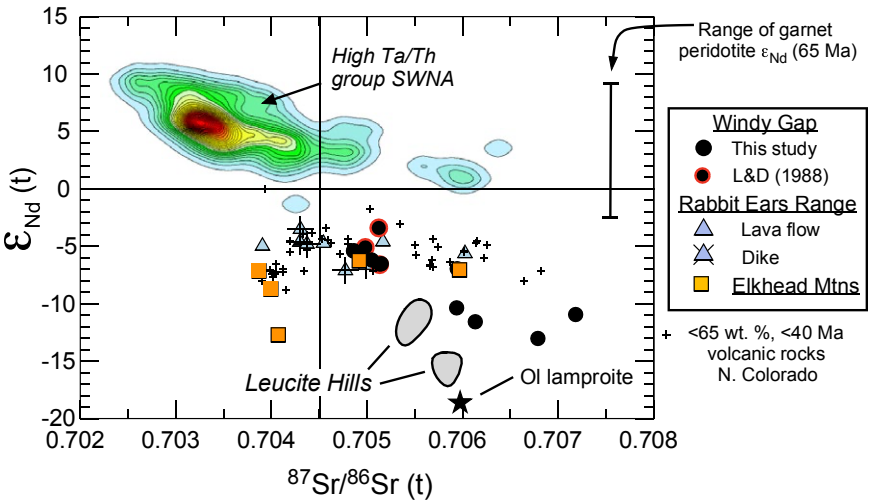

Figure 9. Whole-rock $\varepsilon_{Nd}(t)$ vs. $^{87}Sr/^{86}Sr(t)$ for volcanic rocks in north-central Colorado, USA. Data from late Cenozoic lamproites at Leucite Hills in south-central Wyoming, USA, are from Mirnejad and Bell (2006). Range of isotopic compositions of high Ta/Th (>0.6) group basalts from southwestern North America (SWNA) is from Farmer et al. (2020) and is shown as a smoothed two-dimensional histogram (Eilers and Goeman, 2004). Olivine (Ol) l amproite data (star) are from Thompson et al. (1997). Range of ε_{Nd} values at 65 Ma for garnet peridotite xenoliths in State Line kimberlites is from Carlson et. al. (2004). L&D—Larson and Drexler (1988).

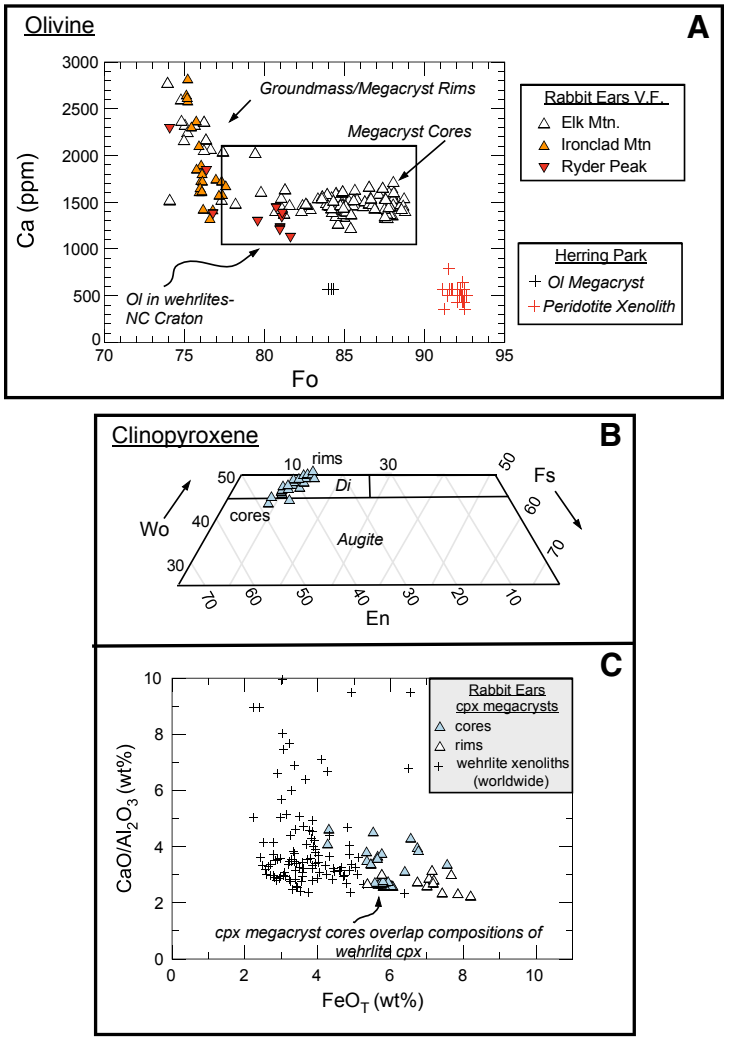

Figure 10. Megacryst compositions from Rabbit Ears volcanic field. (A) Ca (ppm) vs. olivine (Ol) forsterite (Fo) contents for megacrysts and matrix olivine grains from Rabbit Ears volcanic field (V.F.) and for olivine in wehrlite from North China (NC) craton from Lin et al. (2020). (B) Clinopyroxene (cpx) megacryst compositions plotted on pyroxene quadrilateral diagram (Wo—wollastonite; En—enstatite; Di—diopside). (C) Clinopyroxene CaO/Al_2O_3 (wt%) vs. FeO_T (wt%). Compositions of wehrlite clinopyroxene worldwide are from Aulbach et al. (2020).

and trace-element patterns similar to those of island-arc basalts, including low large ion lithophile element (LILE)/high field strength element (HFSE) values and high relative Pb abundances (Kelemen et al., 2014; see also Figs. 6–9). These characteristics apply even to the most compositionally primitive sample (highest wt% MgO ~6.5; 04CO-WG-2C), which is the sample that most closely approximates the composition of primary mantle–derived melts generated during the Laramide orogeny. The isotopic and trace-element compositions of the Windy Gap volcanic cobbles also resemble those of the Table Mountain shoshonitic lava flows (Millikin et al., 2018; Musselman, 1987), which suggests that mafic magmas generated in the northeastern portion of the Colorado Mineral Belt had these characteristics in common. It is not possible to demonstrate that similar mafic magmatism affected the remainder of the Colorado Mineral Belt because so few Laramide-age volcanic rocks are preserved elsewhere (Mutschler et al., 1987), but some Late Cretaceous to early Cenozoic Colorado Mineral Belt silicic intrusive rocks bear evidence that mafic magmatism was involved in their generation. For example, the ca. 67 Ma Whitehorn granodiorite in the Mosquito Range in central Colorado (Fig. 1) contains abundant mafic enclaves and is bordered by an extensive syenogabbro lithologic unit (Abbey et al., 2018; Wrucke, 1974). These mafic lithologies are consistent with the possibility that mafic, presumably mantle-derived, magmas were generally present throughout the Colorado Mineral Belt, even if the silicic igneous rocks that delineate the Colorado Mineral Belt today were themselves the products of lower-crustal anatexis (Stein and Crock, 1990).

The data from the post–40 Ma volcanic rocks demonstrate that high-magnesium (>8 wt% MgO), mantle-derived rocks occur in both the Elkhead and Rabbit Ears volcanic fields, as in other extension-related volcanic areas in north-central Colorado (Gibson et al., 1991; Leat et al., 1988a). In addition, the new eruptive ages from the Rabbit Ears volcanic field confirm that a hiatus of ~30 m.y. separated the older syncompressional and younger synextensional mafic volcanism in this region (Fig. 3D).

Where and why mantle melting occurred during the two volcanic episodes remains to be established. The new and previously published compositional data indicate that mafic volcanic rocks throughout this region have similar alkaline bulk compositions, low $\varepsilon_{Nd}(t)$ (<0), and $^{87}Sr/^{86}Sr$ values from ~0.7045 to 0.707, regardless of age (Figs. 4, 8, and 9). However, rocks from the two episodes have consistently different whole-rock trace-element compositions. The Laramide volcanic rocks all have high LILE/HFSE values; low chondrite-normalized La/Yb values ($[La/Yb]_N$ ~20); prominent spikes in Pb contents; and low Ta, Nb, and Ti abundances on normalized trace-element plots (Figs. 7 and 12). These rocks can be classified as low Ta/Th group (<0.2) volcanic rocks, a compositional grouping recognized for mafic volcanic rocks throughout southwestern North America as described in more detail below (Fig. 13; Farmer et al., 2020). Post–40 Ma mafic rocks, including those from the Rabbit Ears volcanic field, have higher HFSE abundances, higher and more variable $(La/Yb)_N$ (~10–40), lower Pb contents, and higher and more variable Ta/Th values. The contrasts between the two volcanic episodes are reinforced by consideration of published data from both volcanic episodes, which clearly demonstrate

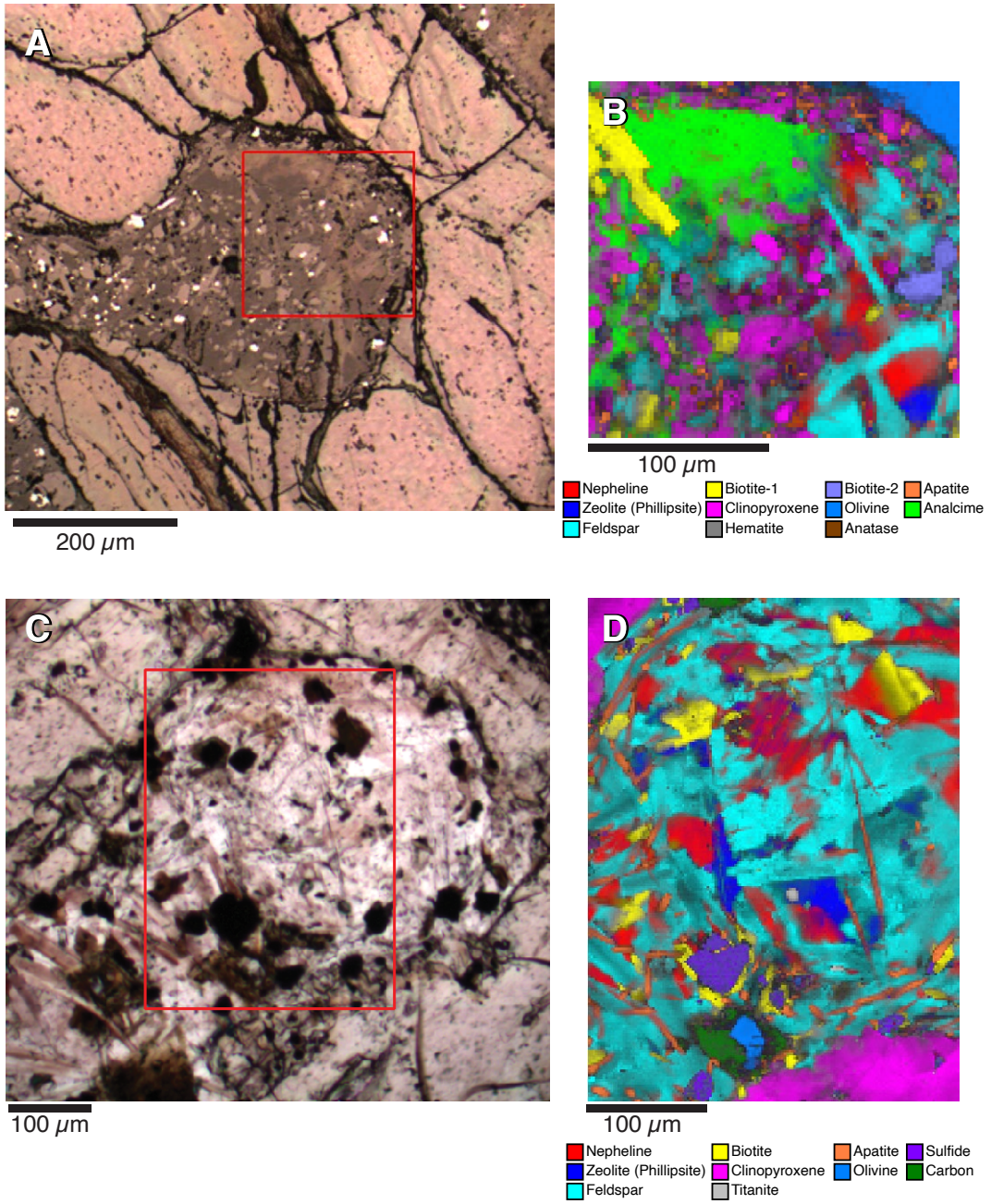

Figure 11. (A–D) Micro-Raman maps of olivine (A, B; sample 18CO-EM-10c) and clinopyroxene (C, D; sample 18CO-EM-10e) megacrysts in dike sample from near Elk Mountain in Rabbit Ears volcanic field. Raman spectra for both melt pockets are available in Supplemental Material Figure S1 (see text footnote 1).

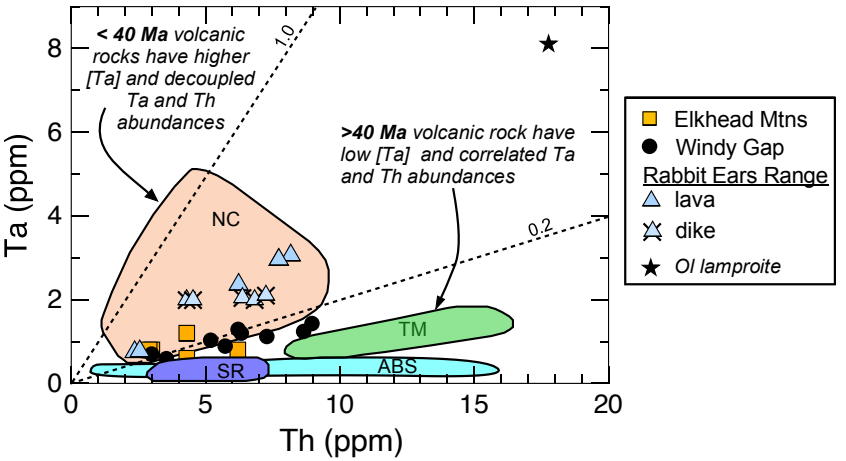

Figure 12. Whole-rock Ta (ppm) vs. Th (ppm) for <65 wt% SiO_2 Cenozoic volcanic rocks in northern Colorado, Wyoming, and SW Montana, USA. TM—Table Mountain (Colorado); ABS—Absaroka volcanic field (Wyoming/Montana); SR—Sliderock volcanic field; NC—northern Colorado; Ol—olivine. Data for northern Colorado are from this study and from Gibson et al. (1991), Knox (2005), Leat et al. (1990), Millikin et al. (2018), and Thompson et al. (1993, 1997). Data for Absaroka volcanic field are from Feeley and Cosca (2003), Feeley et al. (2002), and Lindsay and Feeley (2003), and data for Sliderock Mountain, Montana, are from Farmer (2022).

the higher variances in Ta/Th and $(La/Yb)_N$ values of the post–40 Ma volcanic rocks (Figs. 12–15). The main exceptions are the volcanic rocks from the Elkhead Mountains volcanic field, which have low Ta/Th values similar to older volcanic rocks but the higher $(La/Yb)_N$ values (~22 vs. ~10) characteristic of the younger volcanic rocks (Figs. 6, 7, 12, and 13).

The compositional differences between pre– and post–40 Ma mafic volcanic rocks suggest that the mantle sources of Cretaceous and younger mafic magmatism in north-central Colorado were isotopically similar but imparted different trace-element characteristics to mafic melts as a function of time and tectonic setting. However, such a conclusion requires that the different chemical characteristics of these rocks were inherited from their mafic parental melts and were not imposed by crustal contamination during their ascent to the surface.

Role of Crustal Contamination

Assessing the role of crustal contamination is complicated by postemplacement alteration of our samples as evidenced by high loss on ignition (LOI) values (≤4.6%; Table 2). Alteration could have modified the whole rock wt% P_2O_5/wt%

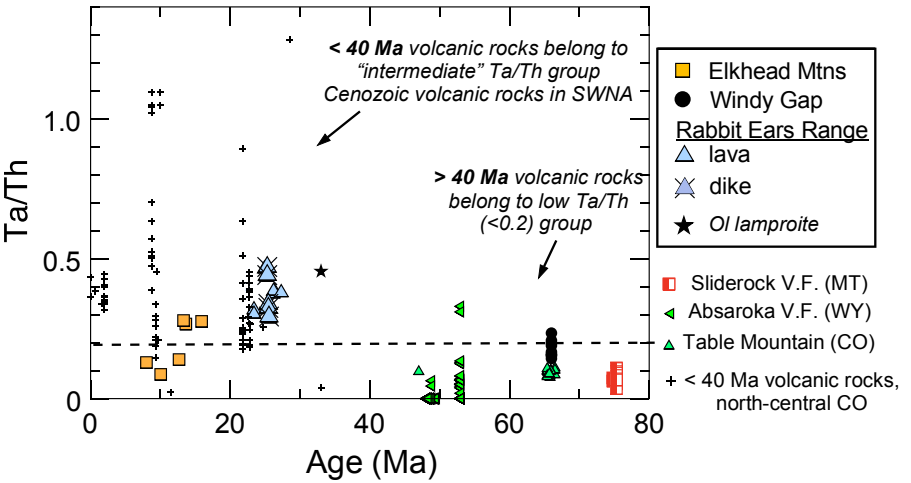

Figure 13. Whole-rock Ta/Th vs. eruptive age for <65 wt% SiO_2 Cenozoic volcanic rocks in northern Colorado (CO), Wyoming (WY), and SW Montana (MT), USA. Data are from sources compiled in Farmer et al. (2020) and in references listed in Figure 12. SWNA—southwestern North America; V.F.—volcanic field; Ol—olivine.

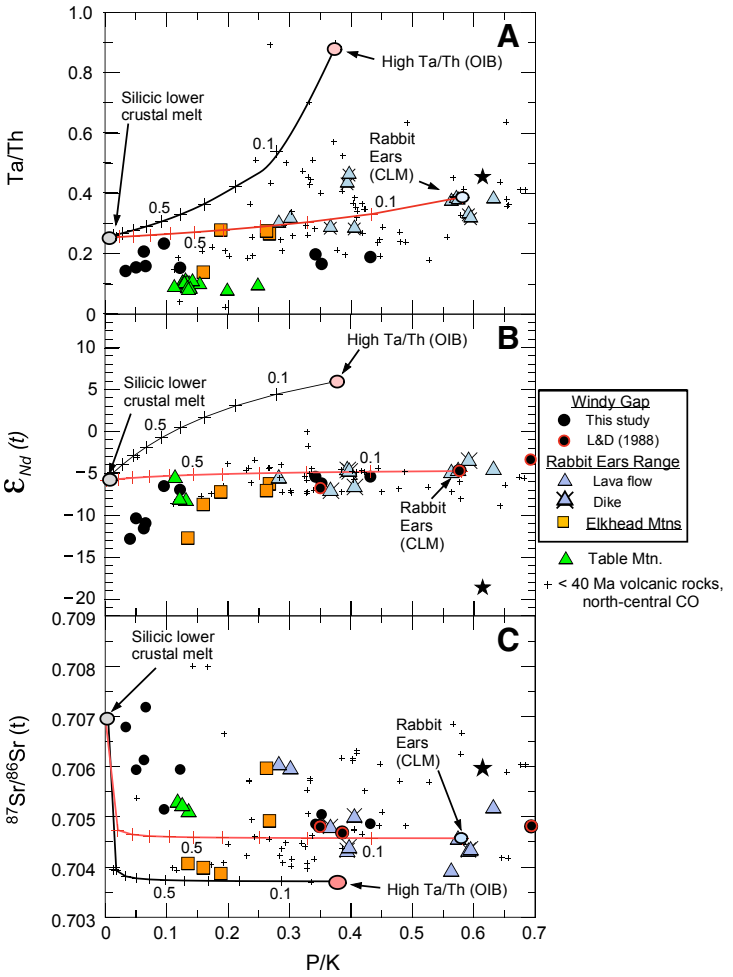

Figure 14. (A–C) Whole-rock P_2O_5/K_2O (P/K; wt%) vs. Ta/Th (A), $\varepsilon_{Nd}(t)$ (B), and $^{87}Sr/^{86}Sr(t)$ (C) for north-central Colorado (CO), USA, volcanic rocks. Simple mixing curves are shown for mixing of average high Ta/Th basalts in southwestern North America (Farmer et al., 2020) and from a representative sample from the Rabbit Ears volcanic field (06CO-PG-11) vs. silicic anatectic melts identified in Never Summer volcanic field (Jacob et al., 2015). Tick marks are 10% increments in mass of silicic end member in mixtures. L&D—Larson and Drexler (1988); OIB—ocean-island basalt; CLM—continental lithospheric mantle.

K_2O value (hereafter referred to as P/K value), which is a commonly used index of upper-crustal contamination, considering that phosphorus and potassium are mobile in mafic volcanic rocks during low-temperature weathering (Carlson and Hart, 1987; Horton, 2015; Eggleton et al., 1987). In contrast, Nd, Ta, and Th are relatively immobile during surficial basalt weathering, and alteration should have little effect on whole-rock Nd isotopic compositions or Ta/Th values (Aiuppa et al., 2000; Kurtz et al., 2000). In the following paragraphs, we emphasize the use of both of these parameters in addressing crustal contamination.

Assimilation of local intermediate- to felsic-composition Paleoproterozoic crust in north-central Colorado by ascending asthenosphere-derived mafic magmas produced solely by upwelling and decompression melting should result in volcanic rock suites in which $\varepsilon_{Nd}(t)$ and Ta/Ta values decrease and $^{87}Sr/^{86}Sr(t)$ values increase with decreasing P/K or wt% MgO (Fig. 14; Carlson and Hart, 1987; Farmer et al., 2020). We base this assertion on low ε_{Nd}(28 Ma) values of Precambrian upper crust in northern Colorado (<–10; DePaolo, 1981), and on the high Ta/Th values, high $\varepsilon_{Nd}(t)$ values (>0), and high P/K values (~0.4) of asthenosphere-derived late Cenozoic basalts found elsewhere in southwestern North America, including those in the southern Rio Grande rift directly south of our field area (Farmer et al., 2020). The lack of consistent variation between whole-rock bulk compositions of our samples and Ta/Th or $\varepsilon_{Nd}(t)$ values argues against the possibility that their parental magmas interacted significantly with the upper crust (Fig. 14). The only possible exceptions are the lowest P/K volcanic rocks from the Laramide Windy Gap Volcanic Member, which have lower $\varepsilon_{Nd}(t)$ and higher $^{87}Sr/^{86}Sr(t)$ values than the rest of the rocks analyzed from this unit.

Interaction between lower continental crust and asthenosphere-derived mafic magmas is also possible, and in north-central Colorado, the lower crust is known to consist of a 15-km-thick section of mafic granulites, based on crustal xenolith populations found in the State Line diatremes (Bradley and McCallum, 1984). Further, geochemical studies of ca. 28 Ma shallow mafic- to silicic-composition igneous rocks in Braddock Peak igneous complex, just to the east of the Rabbit Ears volcanic field (Fig. 2), show that interaction between the lower crust and ascending mafic melts did occur but via mixing between these melts and near-contemporaneous silicic-composition melts that were themselves either directly or indirectly the products of anatexis of mafic lower continental crust (Jacob et al., 2015). We restrict our assessment of potential lower-crustal interaction to processes consistent with these observations. For example, simple mixing between asthenosphere-derived melts and anatectic melts of local, mafic continental crust produces steep arrays in Sr and Nd isotopic compositions and Ta/Th versus P/K, unlike the modest changes in these parameters observed for most of our samples of the Laramide orogeny and post–40 Ma volcanic rocks (Fig. 14). Shallower arrays akin to those observed in our data set can be generated by mixing between the silicic-composition melts and mafic melts if the latter are already characterized by low $\varepsilon_{Nd}(t)$ values and high P/K values similar in composition to the most mafic volcanic rocks in the Laramide and post–40 Ma volcanic episodes (Fig. 14). However, these arrays do not require crustal interaction. The arrays are essentially indistinguishable

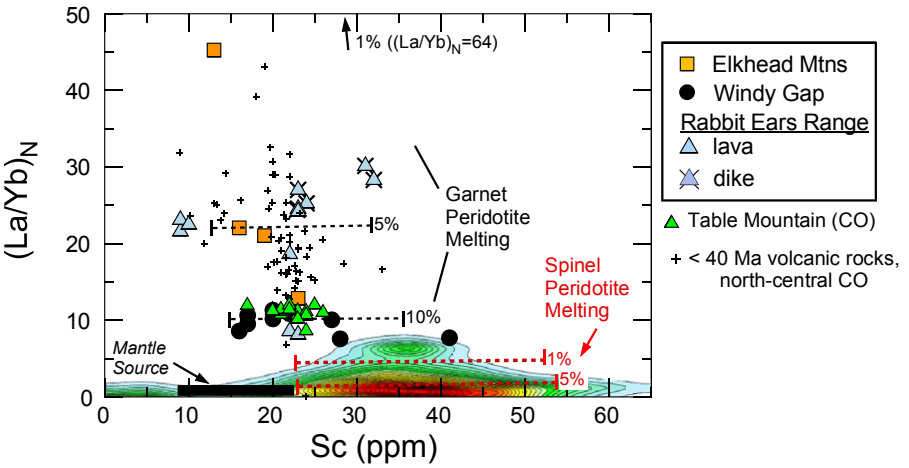

Figure 15. Chondrite-normalized La/Yb values vs. whole Sc abundances for north-central Colorado (CO), USA, volcanic rocks. Dashed lines are calculated ranges of $(La/Yb)_N$ and Sc (ppm) from continental lithospheric mantle source rocks (black), either in garnet stability field (black) or spinel (red). Model parameters are given in Supplemental Material File S5 (see text footnote 1). Ranges of values for island-arc basalts (MgO > 6 wt%) in precompiled GEOROC data sets from Bonin-Izu, New Hebrides, and Kurile Island arcs (colored areas at bottom of plot) are shown for comparison.

from those produced by crystal fractionation in a system closed to crustal interaction, if, for example, a phosphorus-rich phase, such as apatite, were removed from the mafic parental melts during differentiation (Farmer et al., 2020). Overall, we conclude that, with the exception of the lowest P/K samples, the younger and older volcanic rock suites have retained the chemical and isotopic compositions of their parental magmas, unmodified by crustal interaction during ascent and eruption.

Magmatic Models

Our main concern is to determine how mantle melting was generated periodically in an area underlain by Precambrian lithosphere that had been previously amagmatic over a billion years and that extended to depths as great as 200 km prior to the Laramide orogeny. Several general observations are useful in developing plausible models of mantle melt generation. First, low $\varepsilon_{Nd}(t)$ values for continental basalts in southwestern North America are generally attributed to melting or extensive interaction with low $\varepsilon_{Nd}(t)$ ultramafic lithologies in the continental lithospheric mantle (Farmer, 2022; Menzies et al., 1983). We interpret the Nd isotopic composition of mafic volcanic rocks in north-central Colorado in a similar fashion—a conclusion that is supported by the Nd isotopic compositions of fertile, LREE-enriched Paleoproterozoic garnet peridotites from the State Line kimberlites, which also have low ε_{Nd}(28 Ma) values ranging from ~0 to values as low ~–3 (Fig. 9; Carlson et al., 2004). Given the proximity of north-central Colorado to the southern margin of the Archean Wyoming craton (Fig. 1), it is also possible that lower $\varepsilon_{Nd}(t)$ values (<–10) observed for a few of our analyzed rocks, such as those from the Elkhead Mountains volcanic field (Fig. 9), were inherited from Archean continental lithospheric mantle with lower ε_{Nd}. A source in Archean continental lithospheric mantle has been proposed for late Cenozoic lamproites in the Leucite Hills just northwest of our study area in the Wyoming craton of southern Wyoming (Fig. 3D) to account for $\varepsilon_{Nd}(t)$ values ranging from –10 to ~–18 (Fig. 9; Mirnejad and Bell, 2006). With our limited data set, we cannot further address the possibility that Archean lithosphere extends beneath portions of north-central Colorado, although previous workers have suggested from xenoliths in the northernmost State Line diatremes that the base of the continental lithospheric mantle in this region is Archean in age (Eggler et al., 1988), and a 33 Ma olivine lamproite in north-central Colorado has a Nd isotopic composition similar to those of its Leucite Hills counterparts (Figs. 2 and 9; Thompson et al., 1997).

Second, select trace-element abundances of mafic volcanic rocks from both igneous episodes require residual garnet in their mantle sources. This constraint can be illustrated by combined whole-rock $(La/Tb)_N$ values and Sc abundances, because both parameters are affected by the preferential incorporation of HREEs into residual garnet (Fig. 15; Chassé et al., 2018; Wood et al., 2013). Robust forward modeling of melting of continental lithospheric mantle beneath north-central Colorado is handicapped by the lack of comprehensive trace-element data from the State Line xenoliths, but published REE patterns for both garnet and spinel peridotites do exist (Eggler et al., 1988). The latter suggest that most peridotites have low, approximately chondrite, REE abundances and $(La/Yb)_N$ values of ~1. Using these estimated REE concentrations along with whole-rock Sc abundances in the range expected for the upper mantle worldwide (9–22 ppm; Chassé et al., 2018) and representative peridotite mineral modes for the continental lithospheric mantle from xenoliths in the State Line kimberlites (Florence, 1986), and applying nonmodal melting models of spinel and garnet peridotite from the literature (Kinzler, 1997; Walter, 1998), we can generate estimated $(La/Yb)_N$ and Sc abundances of partial melts of continental lithospheric mantle spinel and garnet peridotite (see

Supplemental Material File S5 for more detail on model parameters). These calculations indicate that partial melting of spinel peridotite produces lower $(La/Yb)_N$ and higher Sc abundances (>30 ppm) than observed in our samples. In contrast, melting in the garnet peridotite stability field, with garnet as a residual phase, results in high $(La/Yb)_N$ (≥10) and lower Sc abundances (<30 ppm), matching the characteristics of both the Laramide and post–40 Ma volcanic rocks. At near-solidus temperatures, garnet peridotite is only stable in the upper mantle at depths of 75 km or more, which gains significance in the face of the xenolith evidence showing that the pre-Laramide continental lithospheric mantle extended to depths of at least 200 km. Even if thinned by a factor of two through the course of the Cenozoic, this keel should still restrict any mantle melting to peridotites in the garnet stability field, whether melting occurs in the asthenosphere or at the base of the overlying continental lithospheric mantle. The trace-element data from both volcanic episodes support this expectation. The higher $(La/Yb)_N$ of the post–40 Ma rocks may also be significant because $(La/Yb)_N$ values increase with decreasing extent of partial melting for a given mantle composition (Fig. 14), and models for the origin of the mafic magmatism must also take this observation into account.

Finally, models for the generation of the magmatism must account for not only the chemical differences between mafic rocks, but also for the 30 m.y. hiatus that separates the two magmatic episodes. For this reason, we do not consider models that invoke an ad hoc increase in the potential temperature of the asthenosphere impinging on the base of the preexisting continental lithospheric mantle (e.g., a plume) starting in the Late Cretaceous. Given the thickness of the lithosphere, melting in the upwelling asthenosphere would likely be suppressed, although melting of the base of the continental lithospheric mantle could be triggered in this fashion. However, "instantaneous" basal heating of, and subsequent conductive heat transport through, the continental lithospheric mantle provides no obvious explanation for the 65 m.y. duration of mafic magmatism, punctuated by a 30-m.y.-long hiatus, or an explanation for the distinctly different trace-element compositions of the Laramide and post–40 Ma volcanic rocks.

Relationship to Regional Volcanism in Southwestern North America

Our approach to modeling magma generation in north-central Colorado is to consider these volcanic rocks in the context of extant models for Late Cretaceous and younger magmatism developed elsewhere in southwestern North America, particularly in the southern Basin and Range and the southern Rio Grande rift, which are also areas underlain by Paleoproterozoic continental lithosphere (Fig. 1; Whitmeyer and Karlstrom, 2007). In these regions, Laramide magmatism occurs as a roughly NW-SE–trending belt as far inboard as southernmost New Mexico by ca. 75 Ma (Fig. 1), at which time the magmatism apparently migrated back toward the west (Gilmer et al., 2003; Valencia-Moreno et al., 2017; González-León et al., 2017; Amato et al., 2017). This contrasts with areas immediately to the north, in northern Arizona (USA), New Mexico (USA), and Colorado, where Laramide magmatism was sparse and is mainly represented by the Colorado Mineral Belt (Axen et al., 2018). The southern Basin and Range was then affected by regional a mid-Cenozoic intermediate- to silicic-composition ignimbrite flareup (Lipman and Glazner, 1991) and by the ongoing late Cenozoic, dominantly basaltic, volcanism accompanying lithospheric extension throughout the Basin and Range Province and the Rio Grande rift (Leeman and Rogers, 1970; Baldridge et al., 1995).

A large chemical and isotopic data set is available for volcanic rocks in the southern Basin and Range that provides the basis for detailed models for the origin of space-time-composition patterns in magmatism (Coney and Reynolds, 1977; Glazner, 2022). A useful method of distilling these data, however, is through the relative abundances of Ta and Th, which allow transitions in the compositions of volcanism to be clearly recognized (Farmer et al., 2020). These two elements were chosen for this purpose because they are two of only a few trace elements that are concentrated in the accessory mineral "carrier phases" that can precipitate from aqueous fluids ascending and cooling in continental lithospheric mantle undergoing modal metasomatism: Ta in titanate phases, such as rutile, and Th into the phosphate phase apatite. This is relevant because of the growing evidence that the deep continental lithosphere in inboard areas of southwestern North America underwent extensive aqueous metasomatism coincident with the Laramide orogeny by fluids derived from dewatering of shallowly subducted oceanic lithosphere of the Farallon plate (Apen et al., 2024; Butcher et al., 2017). Hydration of the continental lithospheric mantle in this fashion would lower the mantle solidus temperature, but cooling by the subducted plate would suppress in situ melting of the metasomatized continental lithospheric mantle until such time as the oceanic lithosphere was removed from the base of the lithosphere, and the continental lithospheric mantle was reheated by upwelling asthenosphere (Farmer et al., 2008). Mafic melts derived from continental lithospheric mantle in which metasomatic rutile (rt) ± ap phases have precipitated can be recognized because both carrier phases are solidus phases that deliver their full complement of these elements to melts generated as the metasomatized continental lithospheric mantle is heated. Cenozoic volcanic rocks with variable Ta/Th ranging from 0.2 to 0.6 are common in the southern Basin and Range and include Southern Cordillera Basaltic Andesites (Cameron et al., 1989), which are interpreted as the products of partial melting of metasomatized continental lithospheric mantle (Farmer et al., 2020). These rocks likely owe their variable and "intermediate" Ta/Th values (and their relatively high and variable wt% TiO_2 and wt% P_2O_5 values) to variations in the masses of accessory carrier phases originally present in their metasomatized mantle source rocks (Farmer et al., 2020).

A critical feature for our purposes is that "intermediate"-Ta/Th group volcanic rocks in many locations were emplaced following "low"-Ta/Th basaltic volcanism (Ta/Th ≤ 0.2) and, in some regions, preceded younger, "high"-Ta/Th group volcanism (Ta/Th ~ 1). Low Ta/Th group rocks, such as Late Cretaceous volcanic rocks in inboard regions of the southern Basin and Range (Fig. 1), have high LILE/HFSE values and high relative abundances of Pb, which, along with uniformly low Ta/Th values and wt% TiO_2 < ~1, are characteristic features of island-arc basalts worldwide (Lawton and McMillan, 1999). Despite occurring

far inboard in the continent, these rocks are interpreted to have formed by flux melting of an asthenospheric wedge above subducting and actively dehydrating oceanic lithosphere, as in any arc setting (Amato et al., 2017; Kelemen et al., 2014), presumably contemporaneous with hydrous metasomatism of the overlying continental lithospheric mantle. High-Ta/Th group rocks correspond to late Cenozoic sodic basalts with trace-element characteristics equivalent to those of ocean-island basalts (OIBs), including high Ta/Th values and wt% TiO_2 > ~2 (Figs. 15 and 16); these rocks are the products of decompression melting of passively upwelling asthenospheric mantle as the continental lithospheric mantle progressively thinned during Basin and Range and Rio Grande rift extension (Leeman and Rogers, 1970; Putirka and Platt, 2012). The upshot is that Ta/Th values provide a ready means to track the transition from flux melting of asthenosphere to melting of metasomatized continental lithospheric mantle and then to melting of upwelling "dry" asthenosphere as functions of time and geographic position.

Volcanic rocks in north-central Colorado are not divorced compositionally from those found elsewhere in southwestern North America. Laramide volcanic rocks have trace-element characteristics similar to those of low Ta/Th group rocks, and post–40 Ma rocks are similar compositionally to the intermediate Ta/Th group (Figs. 12 and 13). As a result, the model developed for magmatism in the southern Basin and Range and vicinity should be relevant to understanding the origin of mafic magmatism in north-central Colorado.

Laramide Magmatism in North-Central Colorado

Based on the regional model described in the previous section, the characteristically low Ta/Th values of the Laramide volcanic rocks imply that their parental melts were in fact the products of partial melting of asthenosphere above the actively subducting and dewatering Farallon plate, as some previous workers have suggested (Lipman, 1980; Millikin et al., 2018). This option is still difficult to reconcile with the distance from the trench at which the volcanism occurred, the great thickness of continental lithospheric mantle prior to the Laramide orogeny, and the orientation of Colorado Mineral Belt magmatism (Fig. 17; Chapin, 2012; Jones et al., 2011; Mutschler et al., 1987). Nevertheless, flux melting of asthenosphere actually may have been the most viable method of producing mantle melting beneath this segment of thick mantle lithosphere during the Laramide orogeny. Reduction in the mantle solidus temperature produced upon hydration provides a means of circumventing the effect of a thick lithosphere lid in suppressing melting of upwelling dry asthenosphere (Sarafian et al., 2017). We also note that characteristics of island arcs worldwide include low $(La/Yb)_N$ and higher Sc abundances (>30 ppm), consistent with melting of spinel peridotite at shallow depths in the upper mantle (Fig. 15). The higher $(La/Yb)_N$ values and lower Sc abundances for the Laramide volcanic rocks imply melting in the deeper garnet stability field, which is an expected consequence of flux melting of asthenosphere beneath thick continental lithosphere. The HREE abundances in these rocks essentially constitute a "lid effect" analogous to the effect proposed for the compositions of continental basalts generated solely through decompression melting of dry asthenosphere (Niu, 2021).

An explanation for the orientation of Colorado Mineral Belt magmatism remains elusive, particularly given that Laramide-age, low Ta/Th volcanism in the southern Basin and Range in southern New Mexico and northern Mexico defines a linear belt perpendicular to plate motion, as observed for oceanic and continental margin arcs (Figs. 1 and 17A; Amato et al., 2017; González-León et al., 2017; Lawton and McMillan, 1999). Several models have been proposed to

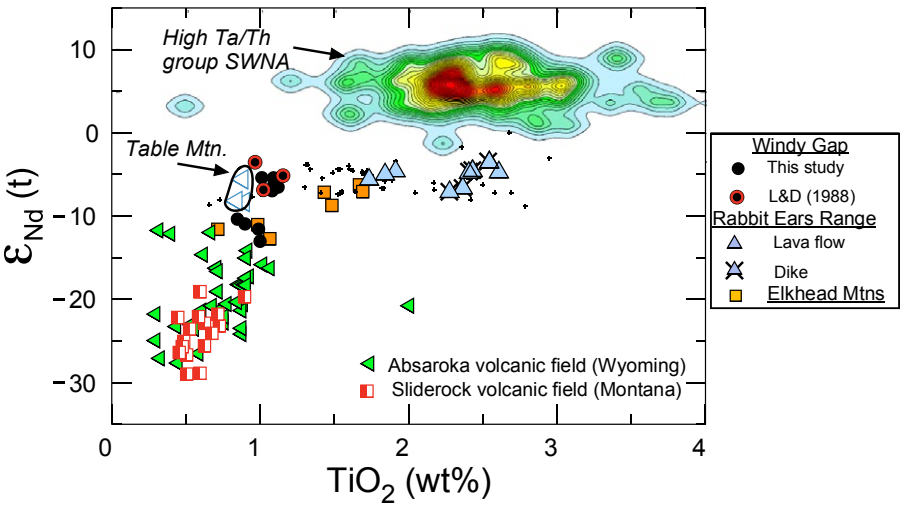

Figure 16. Whole-rock $\varepsilon_{Nd}(t)$ vs. TiO_2 (wt%) for <65 wt% SiO_2 Late Cretaceous and younger volcanic rocks in north-central Colorado, Wyoming, and southern Montana, USA. Sliderock Mountain volcanic field data are from Farmer (2022), Absaroka volcanic field data are from Feeley (2003), Feeley and Cosca (2003), Feeley et al. (2002), and Lindsay and Feeley (2003), and Table Mountain, Colorado, data are from Musselman (1987). L&D—Larson and Drexler (1988); SWNA—southwestern North America.

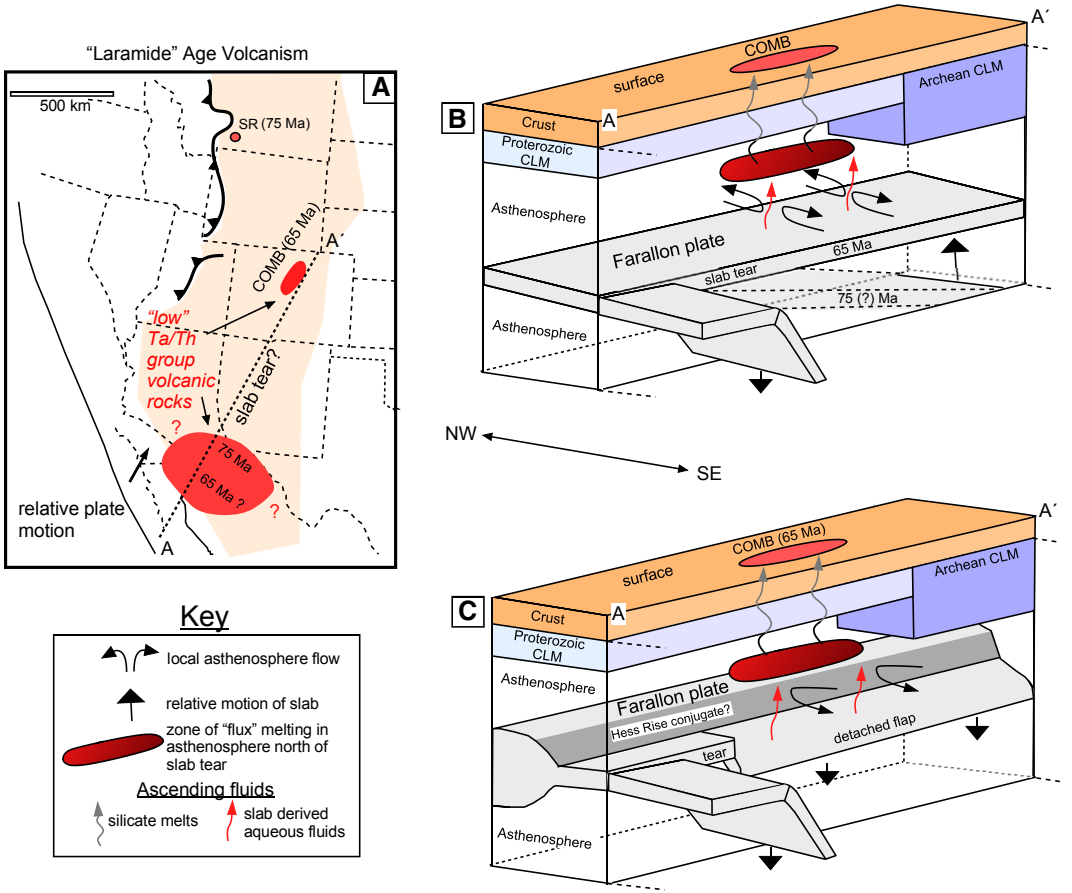

Figure 17. Cartoons illustrating possible scenarios for producing Laramide magmatism via flux melting of asthenosphere beneath Colorado Mineral Belt (COMB). (A) Palinspastic base map shows known distribution of low Ta/Th volcanic rocks (red shaded areas) from southwest North America (SWNA), from 75 Ma to 65 Ma. A wider area than is shown was likely affected by Laramide magmatism (red question marks), but Ta/Th values are unavailable elsewhere for any preserved volcanic rocks in this age range. Light-brown shaded area is approximate extent of Laramide crustal deformation, and hachured line is eastern extent of thin-skinned deformation associated with earlier Sevier orogeny (Jones et al., 2011). SR—Sliderock Mountain volcanic field. (B) Scenario involves flattening of Farallon plate dip angle beneath southwestern North America from 75 Ma to 65 Ma due to interaction of slab with thick Archean lithosphere of Wyoming craton. Secondary convection cells form above slab during flattening, where, with addition of slab-derived fluids, partial melting is localized (after Jones et al., 2011). (C) Scenario shows melting in asthenosphere localized along edge of slab tear in subducting Farallon plate. Embedded in the latter is thick crust corresponding to the Hess Rise conjugate, accounting for shallow dip of subducting slab (after Humphreys et al., 2015). CLM—continental lithospheric mantle.

account for this orientation, all of which invoke a break in the Farallon plate to separate Colorado Mineral Belt magmatism parallel to plate motion from the more steeply dipping portions of the plate to the south above which a trench-parallel continental arc formed (Fig. 17A). One proposed explanation is that the dip angle of the subducting Farallon plate was affected by variations in the thickness of preexisting continental lithosphere, with thicker lithosphere existing beneath the Archean Wyoming craton than the Proterozoic lithosphere to the south (Jones et al., 2011). Interaction between the keel of the Archean continental lithospheric mantle and shallowly subducting oceanic lithosphere of the Farallon plate during the Laramide orogeny could have generated a suction force at the base of the continental lithosphere that induced secondary convection cells parallel to relative plate motion in the asthenosphere as the gap closed between the underthrust oceanic lithosphere and the continental lithospheric mantle through time (Fig. 17B). Decompression melting of the asthenosphere in these cells, however, would not have occurred without thinning of the overlying continental lithosphere, which seems unlikely during a period of lithospheric compression. However, the low Ta/Th characteristics of Laramide magmatism in north-central Colorado imply that hydration of the asthenosphere occurred through dewatering of the Farallon plate (English et al., 2003), which would have permitted melting of upwelling asthenosphere in these secondary convection cells without thinning of the overlying continental lithosphere.

An alternative possibility is that variations in the thickness of the Farallon plate were responsible for the orientation of Colorado Mineral Belt

magmatism (Fig. 17C; Humphreys et al., 2015). This model presumes that a thick but narrow ridge of oceanic crust was embedded in the section of Farallon plate subducted during the Laramide orogeny (Livaccari et al., 1981). The ridge was originally assigned to the conjugate Shatsky Rise, but this ridge likely ceased to interact with the continental margin by 75 Ma, leaving the younger Hess Rise conjugate as the most viable alternative (Schwartz et al., 2023). Colorado Mineral Belt magmatism may have occurred along the southern margin of the subducted Hess Rise conjugate, along a break in the Farallon plate that separated the shallowly subducting thick oceanic lithosphere from more steeply dipping and thinner oceanic crust to the south (Fig. 17C; Humphreys et al., 2015). The low Ta/Th values of the pre–40 Ma volcanic rocks in north-central Colorado would be consistent with this model if the southern edge of the Hess Rise conjugate lithosphere was able to sink deeper into mantle while still dehydrating and inducing counterflow in the overlying asthenosphere, resulting in a band of magmatism parallel to relative plate motion (Fig. 17C).

In both of the above models, mantle melting is initiated in the asthenosphere and not the continental lithospheric mantle. Because mafic melts generated in the asthenosphere typically have $\varepsilon_{Nd}(t) > 0$ (Hofmann, 1997), such an origin must be reconciled with the low, continental lithospheric mantle–like $\varepsilon_{Nd}(t)$ values of the Laramide volcanic rocks. It is unlikely that the low $\varepsilon_{Nd}(t)$ values were imparted directly to asthenosphere beneath the interior portions of southwestern North America through subduction of low $\varepsilon_{Nd}(t)$, continentally derived material. The Catalina Schist, a tectonic mélange exposed in westernmost southwestern North America, represents material likely subducted in the Late Cretaceous beneath southwestern North America, and this mixture of oceanic lithosphere and continentally derived sedimentary detritus has a range of $\varepsilon_{Nd}(t)$ values in the Cretaceous from ~–3 to +15. However, these values are higher values than those observed for most of the mafic volcanic rocks in north-central Colorado (King et al., 2006). In addition, low Ta/Th group mafic volcanic rocks from throughout the Rocky Mountain region have $\varepsilon_{Nd}(t)$ values that correlate with lithospheric age. Low Ta/Th group (≤1 wt% TiO_2) rocks in the Sliderock and Absaroka volcanic fields, regions underlain by Archean lithosphere, have significantly lower $\varepsilon_{Nd}(t)$ values (–10 to –30) than those from the volcanic rocks that erupted through Paleoproterozoic lithosphere in north-central Colorado (Figs. 13 and 16). We suggest that if the low Ta/Th values for pre–40 Ma volcanic rocks throughout the Rocky Mountain region require initiation of mantle melting in the asthenospheric mantle wedge, even at distances far inboard of the western margin of the continent, then initially produced melts likely had high $\varepsilon_{Nd}(t)$ values (>0) and owe their low $\varepsilon_{Nd}(t)$ values to interaction with overlying continental lithospheric mantle during ascent. This hypothesis requires that the melts acquired the continental lithospheric mantle $\varepsilon_{Nd}(t)$ values while maintaining their original low Ta/Th values, but without any knowledge of the Ta/Th values of the Laramide continental lithospheric mantle, it is not possible to further evaluate whether this is an expected consequence of melt–wall rock interaction at the base of the continental lithospheric mantle (Farmer, 2022).

Oligocene and Younger Magmatism and Intermediate Ta/Th Group Volcanism

Most post–40 Ma mafic volcanic rocks in north-central Colorado, including those from the Rabbit Ears, Yampa, Grand Mesa, and Flat Tops volcanic fields (Figs. 2 and 3; Cosca et al., 2014; Gibson et al., 1991; Leat et al., 1988a), have low $\varepsilon_{Nd}(t)$ ~–5, implying that their parental melts involved low ε_{Nd} portions of the underlying Paleoproterozoic continental lithospheric mantle. Hafnium isotopic data are also available for some post–40 Ma mafic volcanic rocks in this region, and these rocks have low ε_{Hf} values (<0), characterized by higher $\varepsilon_{Hf}(t)$ at a given $\varepsilon_{Nd}(t)$ value compared to the isotopic compositions of OIB (Beard and Johnson, 1997). This isotopic feature is also found among the State Line peridotite xenoliths (Carlson et al., 2004) and further supports a derivation of the post–40 Ma volcanic rocks from the local, pre-Laramide, continental lithospheric mantle

Although the post–40 Ma rocks have Nd isotopic compositions similar to those of older Laramide mafic rocks, they have more variable and generally higher Ta/Th values, inconsistent with the subduction-related mechanism proposed for mantle melting associated with the older, low Ta/Th group volcanic rocks. Instead, we suggest the rocks were derived from metasomatized, rt ± ap–bearing, continental lithospheric mantle, as proposed for intermediate Ta/Th group volcanic rocks elsewhere in southwestern North America. For this scenario, underthrust, actively dewatering oceanic lithosphere of the Farallon plate, must have extended as far inboard into the continent as the Southern Rocky Mountains. The Farallon plate served to cool the base of the lithosphere, which prevented the continental lithospheric mantle from immediately melting upon hydration. Melting only occurred when the underthrust oceanic lithosphere was removed and replaced by upwelling, hotter, asthenosphere (Fig. 18). In situ melting of the continental lithospheric mantle can be readily incorporated into existing models for the origin of post–40 Ma magmatism in north-central Colorado. Previous workers have suggested that the periodic east-to-west migration in the locus of basaltic magmatism from ca. 30 Ma to the present across north-central Colorado, as further corroborated by our new $^{40}Ar/^{39}Ar$ data from the Rabbit Ears and Elkhead Mountains volcanic fields, can be attributed to the east-to-west removal of stranded portions of the Farallon plate along the eastern flank of the Colorado Plateau, either by delamination or through gravitational convective instabilities involving the continental lithospheric mantle and any underlying oceanic lithosphere (Fig. 3; Abbott et al., 2022; Cosca et al., 2014; Mutschler et al., 1987). Similar scenarios have been proposed to explain the inward-migrating patterns of Cenozoic magmatism along the plateau's southern and western margins (Fig. 3; Crow et al., 2011; Golos and Fischer, 2022; van Wijk et al., 2010; Wannamaker et al., 2008). Our contribution is the suggestion that, at least in north-central Colorado, mantle melting occurred in situ in metasomatized lithosphere that remained intact and in place after removal of underlying oceanic lithosphere and not within upwelling asthenosphere.

We consider decompression melting of asthenosphere unlikely because of the great thickness of the continental lithosphere still preserved in north-central

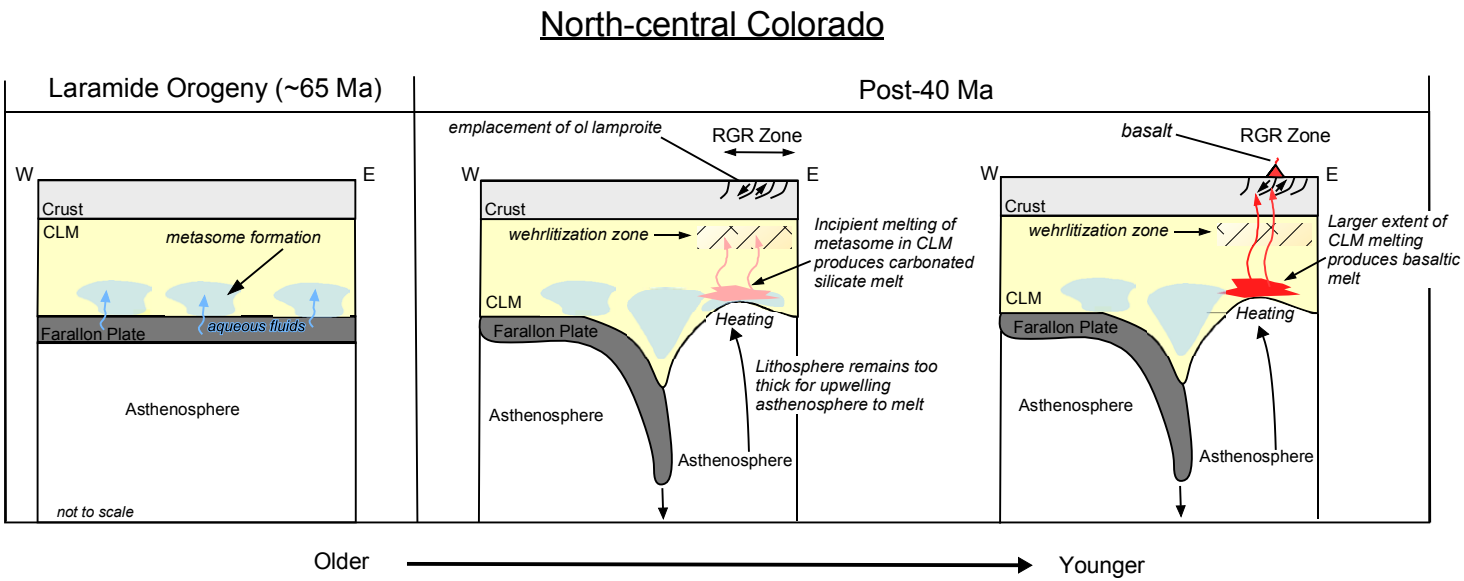

Figure 18. Cartoons showing W-E cross sections through north-central Colorado, USA, starting at left with amagmatic period during Laramide orogeny, when Farallon plate abuts against base of preexisting continental lithospheric mantle (CLM), and then two panels showing onset of post–40 Ma magmatism triggered by removal of remaining Farallon plate remnants from eastern margin of Colorado Plateau. Production and mobilization of carbonated Si-undersaturated melts occur first, along with wehrlitization of shallow continental lithospheric mantle, followed by additional heating and more extensive melting of metasomatized base of continental lithospheric mantle and production of basaltic melts. RGR—Rio Grande rift.

Colorado despite post–40 Ma lithospheric thinning. Based on negative polarity shifts observed from S-wave receiver function analysis, the present-day depth of the lithosphere-asthenosphere boundary is at least 150 km, which remains too thick to allow widespread decompression melting of even damp asthenosphere (Golos and Fischer, 2022; Hansen et al., 2013). Nevertheless, it is possible that narrow regions of thinner continental lithospheric mantle developed during post–40 Ma lithospheric extension in this region that cannot be resolved by seismic methods. The existence of such regions could account for the fact that the highest wt% MgO volcanic rock from the Rabbit Ears volcanic field (~11.6%, sample 06CO-EM-10) yielded equilibration pressures of ~3.2 GPa (~100 km) and temperatures of ~1480 °C for the primary melt parental to this rock, as estimated from major-element thermobarometry algorithms presented by Lee et al. (2009). Equilibration depths determined in this fashion are interpreted to represent the depths at which ascending mafic melts stalled, presumably at the rheologic boundary represented by the lithosphere-asthenosphere boundary (Lee et al., 2009; Plank and Forsyth, 2016). An alternative is that the calculated ~100 km equilibration depth corresponds to a depth wholly within the continental lithospheric mantle. This option is consistent with the negative polarity shift observed at depths of ~100 km to ~60 km, which has been interpreted as a midlithospheric layer of melt accumulation (Hansen et al., 2013).

The estimated melt equilibration temperature is also considerably higher than the ~1300 °C value estimated from seismic data at ~100 km for the lithospheric mantle in north-central Colorado (Hansen et al., 2013). One possible explanation is that the primary melt compositions contained significant amounts of water. Adding 5% H_2O to sample 06CO-EM-10 diminishes the estimated primary melt temperature by over 100 °C while reducing the estimated equilibration depth by ~0.4 GPa (~12 km; Lee et al., 2009). Alternatively, the high calculated melt temperatures could simply reflect temperatures of melts rising from greater depth that remained out of thermal equilibrium with surrounding mantle at their depth of accumulation. In any case, both melt equilibration temperatures and seismic analyses suggest that the temperature at ~100 km beneath north-central Colorado is up to 400 °C hotter than equivalent depths in the High Plains lithosphere to the east (Hansen et al., 2013), consistent with the effect of conductive heating of continental lithospheric mantle in north-central Colorado following removal of remnants of the Farallon plate after 40 Ma.

In situ melting of metasomatized continental lithospheric mantle may also account for the relatively radiogenic and variable $^{87}Sr/^{86}Sr(t)$ values of the

post–40 Ma rocks (Figs. 8, 9, and 14), a feature common to intermediate Ta/Th group volcanic rocks throughout southwestern North America. These Sr isotopic compositions have been attributed to the Sr mobilized in aqueous fluids derived from the subducting Farallon plate, fluids in which the LREEs, including Nd, were relatively immobile (Farmer et al., 2020). The range of whole-rock $^{87}Sr/^{86}Sr(t)$ values could reflect variations in the Sr isotopic compositions of these fluids that were imparted to individual metasomes in the continental lithospheric mantle and then inherited by small-degree melts of the continental lithospheric mantle that rose and erupted independently at the surface. Although speculative, this scenario is at least consistent with the smaller degrees of mantle melting inferred from the high and variable $(La/Yb)_N$ values of the post–40 Ma rocks. In contrast, larger degrees of melting and intermixing of asthenospheric melts prior to or during ascent could account for the lower and more homogeneous $(La/Yb)_N$ values for the Laramide magmatism. The more homogeneous $^{87}Sr/^{86}Sr(t)$ values for the Laramide rocks (~0.705) may also have originated by this mechanism, but like with Nd, it is not possible with the available data to evaluate the role of interaction with continental lithospheric mantle in setting the Sr isotopic composition of their parental melts.

The Elkhead Mountains volcanic field rocks do not fit neatly into the above model because they lack the intermediate Ta/Th values characteristic of all other post–40 Ma rocks in this area, despite having similarly high and variable $(La/Yb)_N$ values (Fig. 15). One possible explanation is that these rocks were derived from lithosphere that had been hydrated during the Laramide orogeny but simply did not acquire a large mass of precipitated accessory carrier phases. Melting at the same general depth in hydrated garnet peridotite would account for the similar $(La/Th)_N$ values and Sc abundances in these and other post–40 Ma rocks, and their higher wt% TiO_2 values compared to the Laramide rocks might indicate that their sources contained at least some titanium-bearing accessory phases, even if less than continental lithospheric mantle farther to the south and east in north-central Colorado (Figs. 5 and 16).

Extensional Tectonism and Magmatism

Although we prefer a model in which post–40 Ma magmatism in north-central Colorado originated through in situ melting of metasomatized continental lithospheric mantle and not melting of asthenosphere under thinned lithosphere, it remains possible that magmatism was synchronous with upper-crustal extension, as is the case along much of the Rio Grande rift system (Baldridge et al., 1995). The link between extension and magmatism is particularly evident in the Rabbit Ears volcanic field, where the volcanic rocks are interbedded with synextensional basin fill (Prothero, 2011; Shroba, 2016; Shroba et al., 2010). Our $^{40}Ar/^{39}Ar$ ages from the Rabbit Ears volcanic rocks restrict the timing of upper-crust extension to the time interval from 27.3 Ma to 23.4 Ma, similar to that determined from apatite U-Th-He studies for the older (ca. 30 Ma) of the two Cenozoic extensional episodes recorded along the east flank of the Gore Range just to the southwest of our study area (Landman and Flowers, 2013).

Although extensional tectonism in north-central Colorado may represent the northern limit of the Rio Grande rift system, this area nevertheless experienced a much smaller degree of extension (<20%) and thinner rift-fill sedimentation (<200 m) than are characteristic of the southern portions of the rift (Kellogg, 1999). As a result, the Rabbit Ears basaltic rocks, which are some of the oldest extension-related volcanic rocks in north-central Colorado, may provide insights into the processes involved in the incipient extension of the thick continental lithosphere.

Megacrysts entrained in basaltic dikes from the Rabbit Ears volcanic field provide one such window into incipient extension of the lithosphere. The fact that the cores of individual ol and clinopyroxene megacrysts are unzoned and the fact that the grains themselves occur as glomerocrysts and individual subhedral grains of various sizes suggest that these crystals are xenocrysts unrelated to their host magmas (Fig. 10; Righter and Carmichael, 1993). Only the higher Ca and lower Mg# rims on both cpx and ol grains are likely the products of equilibration between basaltic host melt and megacrysts after the entrainment of the latter in the ascending basaltic magma. Olivine in equilibrium with a mafic melt similar in compositional to aphyric lavas in the Rabbit Ears volcanic field, such as samples EM-03 or CP-09, should range in composition from ~Fo_{65} to ~Fo_{80}, which are the values observed for ol megacryst rims and groundmass grains in the dike samples (assuming Fe^{2+}-Mg olivine-melt partition of 0.3 and melt $Fe^{2+}/Fe_{total} = 0.9$). These megacrysts are also unlikely to represent disaggregated mantle peridotites. Olivine megacryst cores have lower Mg# (~80–90) and higher Ca contents (~1200 ppm to 1700 ppm) than are typical of grains found in harzburgite or lherzolite grains, including those present in spinel peridotite xenoliths in the ca. 8 Ma Herring Park basalts found south of our study area in South Park, Colorado (Mg# = 91–93; Ca = 300–800 ppm; Figs. 1 and 10A). The latter is the only mantle xenolith locality known in Late Cretaceous and younger basalts in this region (Melton, 2007), and both ol and cpx compositions in the Herring Park basalt xenoliths are similar to those determined in peridotite xenoliths entrained in the Devonian State Line kimberlites (Eggler et al., 1987, 1976). Cpx megacrysts from the Rabbit Ears volcanic field are diopsidic but have lower Mg# (~80) and lower Cr contents (~1400 ppm) than are typical of chromium diopsides derived from disaggregated peridotites (Liu and Ying, 2020).

In contrast, the ol and cpx megacryst core compositions are similar to those of grains comprising wehrlite xenoliths worldwide, although the cpx cores have wt% FeO_T at the extreme high end of the range recognized for wehrlite cpx worldwide (Fig. 10; Aulbach et al., 2020; Lin et al., 2020). Wehrlites can represent ol + cpx cumulates derived from crystallization of basaltic magmas in the lower crust or the products of metasomatism of shallow spinel peridotites and harzburgites via decarbonation reactions with hydrous, carbonated silicate melts during which mantle orthopyroxene transforms into olivine and diopside plus CO_2 vapor (Peters et al., 2016; Weidendorfer et al., 2020). The upward migration of hydrous, carbonate-rich but silica-undersaturated melts, and their interaction with shallow spinel peridotites, is thought to account for the emission of CO_2(g) commonly associated with continental rift zones (Foley and Fischer, 2017).

A metasomatic origin for the Rabbit Ears ol and cpx xenocrysts could account for the lack of orthopyroxene observed in the xenocryst mineral assemblage, if orthopyroxene originally present in the shallow continental lithospheric mantle was completely exhausted along melt conduits during melt–wall rock interaction. Trace-element data from the grains might more definitively distinguish between a cumulate versus metasomatic grains (Kukuła et al., 2015), but in the absence of such, we refer instead to the melt pockets present in both ol and cpx megacrysts, which are common in wehrlites worldwide and support a metasomatic origin for these grains (Loges et al., 2019). The melt pockets we investigated contain 5%–7% nph, which appears to be absent in the matrix of the host basalt (Fig. 11; Supplemental Material Fig. S2), in which case the pockets cannot solely represent infiltration of the host basaltic melt into the xenocrysts after entrainment. An alternative is that nph-bearing domains in the melt pockets represent more silica-undersaturated, alkalic melts of the local continental lithospheric mantle that interacted with the wehrlite veins prior to their entrainment in the host basalts.

The timing of wehrlitization is unknown, other than it predated entrainment in the basaltic magmas at ca. 24 Ma. However, a sodic-composition olivine lamproite was emplaced along the eastern margin of North Park at ca. 33 Ma, some 5 m.y. prior to the onset of the bulk of Oligocene magmatism in this area at ca. 28 Ma (Fig. 2; Thompson et al., 1997). It is possible that the melt pockets also represent silica-undersaturated melts percolating through continental lithospheric mantle in the Oligocene. These melts could have been responsible for the metasomatism related to the formation of the wehrlites themselves (Fig. 18). If wehrlitization was indeed Oligocene in age, then the ol and cpx megacrysts provide indirect evidence that silica-undersaturated, hydrous, and CO_2-rich melts were produced and mobilized early in the process that led to upper-crustal extension by ca. 28 Ma. These melts could represent initial, small-degree partial melting of the continental lithospheric mantle, with later basalts representing the products of later, more-extensive melting of this same source (Fig. 18; Gudfinnsson and Presnall, 2005). The very low $\varepsilon_{Nd}(t)$ values (~–20) for the 33 Ma olivine lamproite (Fig. 14) suggest that this rock may have been derived from a continental lithospheric mantle source with an older age, as discussed in the Magmatic Models section, or one with greater LREE enrichment than the source of the mafic melts parental to the basalts at the Rabbit Ears volcanic field (Thompson et al., 1997).

Overall, we suggest that the production and mobilization of continental lithospheric mantle–derived carbonated silicate melts in north-central Colorado occurred prior to the onset of upper-crustal extension and the post–40 Ma basaltic volcanism, a process that may be a general feature of the early stages of lithospheric thinning in continental rift zones (Foley and Fischer, 2017; Rosenthal et al., 2009). In north-central Colorado, the production of carbonated silicate melts could represent the incipient response of metasomatized continental lithospheric mantle to heating after removal of underlying Farallon plate remnants, with the generation of intermediate Ta/Th group basaltic magmatism following as heating continued (Fig. 18). Elsewhere in southwestern North America, including the southern Rio Grande rift, intermediate Ta/Th group basalts were supplanted through time to the late Cenozoic by high $\varepsilon_{Nd}(t)$ (>0), low $^{87}Sr/^{86}Sr(t)$ (<0.7040), and high Ta/Th group mafic volcanism. The latter has long been attributed to decompression melting of asthenosphere upwelling in response to Basin and Range lithospheric extension and thinning (Farmer et al., 2020; Leeman and Rogers, 1970). The absence of high Ta/Th group mafic volcanic rocks in north-central Colorado is consistent with the conclusion that thick, low $\varepsilon_{Nd}(0)$ continental lithosphere has been preserved here to the present day, even after removal of remnants of Farallon oceanic lithosphere from the base of the continental lithospheric mantle. In those portions of the Basin and Range where the magnitude of late Cenozoic extension and lithospheric thinning is greater, decompression melting of asthenosphere occurred and resulted in the production of high $\varepsilon_{Nd}(t)$ and high Ta/Th group basalts.

CONCLUSIONS

New and existing chemical and isotopic data from Late Cretaceous and younger mafic volcanic rocks in north-central Colorado demonstrate that these volcanic rocks show compositional variations through time similar to those observed for volcanic rocks of similar age throughout southwestern North America. The broad implication is that despite developing far inboard from the western continental margin and in a region underlain by thick Precambrian continental lithosphere, the source regions and trigger mechanisms for mantle melting in north-central Colorado were essentially equivalent to those invoked elsewhere in southwestern North America. The older, syncompressional, low Ta/Th magmatism is best attributed to flux-melting in the asthenosphere above shallowly subducting and dehydrating oceanic lithosphere of the Farallon plate. The primary melts so generated then interacted during ascent with overlying, low $\varepsilon_{Nd}(0)$ mantle lithosphere. Post–40 Ma mafic volcanics rocks are also characterized by lithosphere-derived Nd, but they belong to the intermediate Ta/Th group of volcanic rocks recognized throughout southwestern North America. The latter are attributed to in situ melting of preexisting continental lithospheric mantle that had been cooled and metasomatized because of underplating by the Farallon oceanic lithosphere. Progressive east-to-west removal of this lithosphere during the late Cenozoic along the eastern margin of the Colorado Plateau in north-central Colorado resulted in upwelling of underlying asthenosphere, heating of the remaining continental lithospheric mantle, and the production of intermediate Ta/Th mafic melts. The involvement of continental lithospheric mantle with low $\varepsilon_{Nd}(0)$ in mafic volcanism throughout the Cenozoic is consistent with the preservation of a thick continental lithospheric mantle in this region, even after being affected by both the emplacement and subsequent removal of shallowly subducting oceanic lithosphere. In contrast, much of the Basin and Range experienced greater degrees of extension and lithospheric thinning than the Southern Rocky Mountains in Colorado, which ultimately led to high Ta/Th group mafic volcanism during the late Cenozoic. The lack of high Ta/Th mafic volcanism in north-central Colorado was likely a consequence of the preservation of thick continental lithospheric mantle in this

region, which inhibited decompression melting of upwelling asthenosphere even after removal of stranded remnants of the Farallon plate.

ACKNOWLEDGMENTS

This material is based in part upon work supported by the National Science Foundation under award no. 0810201 to Farmer. The paper was greatly improved by journal reviewers Mary Reid and Josh Schwartz, as well as Associate Editor Eric H. Christiansen. Raman spectroscopy was performed at the Raman Microspectroscopy Laboratory, Department of Geological Sciences, University of Colorado at Boulder (RRID: SCR_019305). The views expressed in this paper are those of the authors and do not necessarily reflect the views or policies of the U.S. Environmental Protection Agency, but they do reflect the views of the U.S. Geological Survey. Any use of trade, product, or firm names is for descriptive purposes only and does not imply endorsement by the U.S. government.

REFERENCES CITED

Abbey, A.L., Niemi, N.A., Geissman, J.W., Winkelstern, I.Z., and Heizler, M., 2018, Early Cenozoic exhumation and paleotopography in the Arkansas River valley, Southern Rocky Mountains, Colorado: Lithosphere, v. 10, no. 2, p. 239–266, https://doi.org/10.1130/L673.1.

Abbott, L.D., Flowers, R.M., Metcalf, J., Falkowski, S., and Niazy, F., 2022, Post-Laramide, Eocene epeirogeny in central Colorado—The result of a mantle drip?: Geosphere, v. 18, no. 4, p. 1223–1246, https://doi.org/10.1130/GES02434.1.

Aiuppa, A., Allard, P., D'Alessandro, W., Michel, A., Parello, F., Treuil, M., and Valenza, M., 2000, Mobility and fluxes of major, minor and trace metals during basalt weathering and groundwater transport at Mt. Etna volcano (Sicily): Geochimica et Cosmochimica Acta, v. 64, no. 11, p. 1827–1841, https://doi.org/10.1016/S0016-7037(00)00345-8.

Amato, J.M., Mack, G.H., Jonell, T.N., Seager, W.R., and Upchurch, G.R., 2017, Onset of the Laramide orogeny and associated magmatism in southern New Mexico based on U-Pb geochronology: Geological Society of America Bulletin, v. 129, no. 9–10, p. 1209–1226, https://doi.org/10.1130/B31629.1.

Apen, F.E., Rudnick, R.L., Flowers, R.M., Gaynor, S.P., and Cottle, J.M., 2024, Metasomatism of the Wyoming craton lower crust during the Laramide orogeny: Extending the record of lithosphere hydration across western North America: Earth and Planetary Science Letters, v. 641, https://doi.org/10.1016/j.epsl.2024.118832.

Artemieva, I.M., and Mooney, W.D., 2001, Thermal thickness and evolution of Precambrian lithosphere: A global study: Journal of Geophysical Research: Solid Earth, v. 106, no. B8, p. 16,387–16,414, https://doi.org/10.1029/2000JB900439.

Aulbach, S., Lin, A.B., Weiss, Y., and Yaxley, G.M., 2020, Wehrlites from continental mantle monitor the passage and degassing of carbonated melts: Geochemical Perspectives Letters, v. 15, p. 30–34, https://doi.org/10.7185/geochemlet.2031.

Axen, G.J., van Wijk, J.W., and Currie, C.A., 2018, Basal continental mantle lithosphere displaced by flat-slab subduction: Nature Geoscience, v. 11, no. 12, p. 961–964, https://doi.org/10.1038/s41561-018-0263-9.

Baldridge, W.S., Keller, G.R., Haak, V., Wendlandt, E., Jiracek, G.R., and Olsen, K.H., 1995, The Rio Grande rift, *in* Olsen, K.H., ed., Continental Rifts: Evolution, Structure, Tectonics (1st ed.): Amsterdam, Netherlands, Elsevier, Developments in Geotectonics Volume 25, p. 233–275, https://doi.org/10.1016/S0419-0254(06)80014-5.

Beard, B.L., and Johnson, C.M., 1997, Hafnium isotope evidence for the origin of Cenozoic basaltic lavas from the southwestern United States: Journal of Geophysical Research: Solid Earth, v. 102, p. 20,149–20,178, https://doi.org/10.1029/97JB01731.

Bradley, S.D., and McCallum, M.E., 1984, Granulite facies and related xenoliths from Colorado-Wyoming kimberlite, *in* Kornprobst, J., ed., Proceedings of the Third Kimberlite Conference: Amsterdam, Netherlands, Elsevier.

Burack Wilson, A., and Sims, P.K., 2003, Colorado Mineral Belt Revisited—An Analysis of New Data: U.S. Geological Survey Open-File Report 03–046, 4 p., https://pubsdata.usgs.gov/pubs/of/2003/ofr-03-046/.

Butcher, L.A., Mahan, K.H., and Allaz, J.M., 2017, Late Cretaceous crustal hydration in the Colorado Plateau, USA, from xenolith petrology and monazite geochronology: Lithosphere, v. 9, p. 561–578, https://doi.org/10.1130/L583.1.

Cameron, K.L., Nimz, G.J., Kuentz, D., Niemeyer, S., and Gunn, S., 1989, The southern Cordilleran basaltic andesite suite, southern Chihuahua, Mexico: A link between Tertiary continental arc and flood basalt magmatism in North America: Journal of Geophysical Research: Solid Earth, v. 94, p. 7817–7840, https://doi.org/10.1029/JB094iB06p07817.

Carlson, R.W., and Hart, W.K., 1987, Crustal genesis on the Oregon Plateau: Journal of Geophysical Research: Solid Earth, v. 92, p. 6191–6206, https://doi.org/10.1029/JB092iB07p06191.

Carlson, R.W., Irving, A.J., Schulze, D.J., Hearn, J., and Carter, B., 2004, Timing of Precambrian melt depletion and Phanerozoic refertilization events in the lithospheric mantle of the Wyoming craton and adjacent Central Plains orogen: Lithos, v. 77, no. 1–4, p. 453–472, https://doi.org/10.1016/j.lithos.2004.03.030.

Carlson, R.W., Pearson, D.G., and James, D.E., 2005, Physical, chemical, and chronological characteristics of continental mantle: Reviews of Geophysics, v. 43, no. 1, RG1001, https://doi.org/10.1029/2004RG000156.

Chantler, C.T., Olsen, K., Dragoset, R.A., Chang, J., Kishore, A.R., Kotochigova, S.A., and Zucker, D.S., 2005, X-Ray Form Factor, Attenuation, and Scattering Tables: National Institute of Standards and Technology (NIST) Standard Reference Database 66, https://doi.org/10.18434/T4HS32.

Chapin, C.E., 2012, Origin of the Colorado Mineral Belt: Geosphere, v. 8, no. 1, p. 28–43, https://doi.org/10.1130/GES00694.1.

Chassé, M., Griffin, W.L., Alard, O., O'Reilly, S.Y., and Calas, G., 2018, Insights into the mantle geochemistry of scandium from a meta-analysis of garnet data: Lithos, v. 310, p. 409–421, https://doi.org/10.1016/j.lithos.2018.03.026.

Cole, J.C., Trexler, J.H.J., Cashman, K., Miller, I.M., Shroba, R.R., Cosca, M.A., and Workman, J.B., 2010, Beyond Colorado's Front Range—A new look at Laramide basin subsidence, sedimentation, and deformation in north-central Colorado, *in* Morgan, L.A., and Quane, S.L., eds., Through the Generations: Geologic and Anthropogenic Field Excursions in the Rocky Mountains from Modern to Ancient: Geological Society of America Field Guide 18, p. 55–76, https://doi.org/10.1130/2010.0018(03).

Coney, P.J., and Reynolds, S.J., 1977, Cordilleran Benioff zones: Nature, v. 270, no. 5636, p. 403–406, https://doi.org/10.1038/270403a0.

Cosca, M.A., Thompson, R.A., Lee, J.P., Turner, K.J., Neymark, L.A., and Premo, W.R., 2014, Ar-40/Ar-39 geochronology, isotope geochemistry(Sr, Nd, Pb), and petrology of alkaline lavas near Yampa, Colorado: Migration of alkaline volcanism and evolution of the northern Rio Grande rift: Geosphere, v. 10, no. 2, p. 374–400, https://doi.org/10.1130/GES00921.1.

Crow, R., Karlstrom, K., Asmerom, Y., Schmandt, B., Polyak, V., and DuFrane, S.A., 2011, Shrinking of the Colorado Plateau via lithospheric mantle erosion: Evidence from Nd and Sr isotopes and geochronology of Neogene basalts: Geology, v. 39, no. 1, p. 27–30, https://doi.org/10.1130/G31611.1.

Dechesne, M., Cole, J.C., Trexler, J.H.J., Cashman, P.H., and Peterson, C.D., 2013, Laramide basin CSI: Comprehensive stratigraphic investigations of Paleogene sediments in the Colorado Headwaters Basin, north-central Colorado, *in* Abbott, L.D., and Hancock, G.S., eds., Classic Concepts and New Directions: Exploring 125 Years of GSA Discoveries in the Rocky Mountain Region: Geological Society of America Field Guide 33, p. 139–163, https://doi.org/10.1130/2013.0033(04).

DePaolo, D.J., 1981, Neodymium isotopes in the Colorado Front Range and crust-mantle evolution in the Proterozoic: Nature, v. 291, no. 5812, p. 193–196, https://doi.org/10.1038/291193a0.

Dickinson, W.R., 2004, Evolution of the North American Cordillera: Annual Review of Earth and Planetary Sciences, v. 32, p. 13–45, https://doi.org/10.1146/annurev.earth.32.101802.120257.

du Bray, E.A., and Harlan, S.S., 1998, Geology, Age, and Tectonic Setting of the Cretaceous Sliderock Mountain Volcano, Montana: U.S. Geological Survey Professional Paper 1602, p. 1–19, https://doi.org/10.3133/pp1602.

Eaton, G.P., 2008, Epeirogeny in the Southern Rocky Mountains region: Evidence and origin: Geosphere, v. 4, no. 5, p. 764–784, https://doi.org/10.1130/GES00149.1.

Eggler, D.H., McCallum, M.E., and Smith, C.B., 1976, Upper mantle nodules in Colorado Wyoming kimberlites: Eos (Transactions of the American Geophysical Union), v. 57, no. 10, p. 761–762.

Eggler, D.H., McCallum, M.E., and Kirkley, M.B., 1987, Kimberlite-transported nodules from Colorado-Wyoming; A record of enrichment of shallow portions of an infertile lithosphere, *in* Mullen-Morris, E., and Dill-Pasteris, J., eds., Mantle Metasomatism and Alkaline Magmatism: Geological Society of America Special Paper 215, p. 77–90, https://doi.org/10.1130/SPE215-p77.

Eggler, D.H., Meen, J.K., Welt, F., Dudas, F.O., Furlong, K.P., McCallum, M.E., and Carlson, R.W., 1988, Tectonomagmatism of the Wyoming Province: Colorado School of Mines Quarterly, v. 83, p. 25–40.

Eggleton, R.A., Foudoulis, C., and Varkevisser, D., 1987, Weathering of basalt—Changes in rock chemistry and mineralogy: Clays and Clay Minerals, v. 35, no. 3, p. 161–169, https://doi.org/10.1346/CCMN.1987.0350301.

Eilers, P.H.C., and Goeman, J.J., 2004, Enhancing scatterplots with smoothed densities: Bioinformatics, v. 20, no. 5, p. 623–628.

English, J.M., Johnston, S.T., and Wang, K.L., 2003, Thermal modelling of the Laramide orogeny: Testing the flat-slab subduction hypothesis: Earth and Planetary Science Letters, v. 214, no. 3–4, p. 619–632, https://doi.org/10.1016/S0012-821X(03)00399-6.

Erslev, E.A., 1993, Thrusts, back-thrusts, and detachment of Rocky Mountain foreland arches, *in* Schmidt, C.J., Chase, R.B., and Erslev, E.A., eds., Laramide Basement Deformation in the Rocky Mountain Foreland of the Western United States: Geological Society of America Special Paper 280, p. 339–358, https://doi.org/10.1130/SPE280-p339.

Evanoff, E., 1990, Early Oligocene paleovalleys in southern and central Wyoming—Evidence of high local relief on the late Eocene unconformity: Geology, v. 18, no. 5, p. 443–446, https://doi.org/10.1130/0091-7613(1990)018<0443:EOPISA>2.3.CO;2.

Farmer, G.L., 2022, Reassessing the role of continental lithospheric mantle in Cenozoic magmatism, southwestern North America, *in* Sims, K.W.W., Maher, K., and Schrag, D.P., eds., Isotopic Constraints on Earth System Science: American Geophysical Union Geophysical Monograph 273, p. 57–86, https://doi.org/10.1002/9781119595007.ch4.

Farmer, G.L., Bowring, S.A., Williams, M.L., Christensen, N.I., Matzel, J.P., and Stevens, L., 2005, Contrasting lower crustal evolution across an Archean-Proterozoic suture: Physical, chemical and geochronologic studies of lower crustal xenoliths in southern Wyoming and northern Colorado, *in* Karlstrom, K.E., and Keller, G.R., eds., The Rocky Mountain Region: An Evolving Lithosphere—Tectonics, Geochemistry, and Geophysics: American Geophysical Union Geophysical Monograph 154, p. 139–162, https://doi.org/10.1029/154GM11.

Farmer, G.L., Bailley, T., and Elkins-Tanton, L.T., 2008, Mantle source volumes and the origin of the mid-Tertiary ignimbrite flare-up in the southern Rocky Mountains, western US: Lithos, v. 102, no. 1–2, p. 279–294, https://doi.org/10.1016/j.lithos.2007.08.014.

Farmer, G.L., Fritz, D.E., and Glazner, A.F., 2020, Identifying metasomatized continental lithospheric mantle involvement in Cenozoic magmatism from Ta/Th values, southwestern North America: Geochemistry, Geophysics, Geosystems, v. 21, no. 5, https://doi.org/10.1029/2019GC008499.

Feeley, T.C., 2003, Origin and tectonic implications of across-strike geochemical variations in the Eocene Absaroka volcanic province, United States: The Journal of Geology, v. 111, no. 3, p. 329–346, https://doi.org/10.1086/373972.

Feeley, T.C., and Cosca, M.A., 2003, Time vs. composition trends of magmatism at Sunlight volcano, Absaroka volcanic province, Wyoming: Geological Society of America Bulletin, v. 115, no. 6, p. 714–728, https://doi.org/10.1130/0016-7606(2003)115<0714:TVCTOM>2.0.CO;2.

Feeley, T.C., Cosca, M.A., and Lindsay, C.R., 2002, Petrogenesis and implications of calc-alkaline cryptic hybrid magmas from Washburn volcano, Absaroka volcanic province, USA: Journal of Petrology, v. 43, no. 4, p. 663–703, https://doi.org/10.1093/petrology/43.4.663.

Florence, F.P., 1986, Petrology of Mantle Xenoliths in the Sloan Kimberlite, Larimer County, Colorado [M.Sc. thesis]: Tucson, Arizona, University of Arizona, 110 p.

Foley, S.F., and Fischer, T.P., 2017, An essential role for continental rifts and lithosphere in the deep carbon cycle: Nature Geoscience, v. 10, no. 12, p. 897–902, https://doi.org/10.1038/s41561-017-0002-7.

Gibson, S.A., Thompson, R.N., Leat, P.T., Morrison, M.A., Hendry, G.L., and Dickin, A.P., 1991, The Flat Tops volcanic field. 1. Lower Miocene open-system, multisource magmatism at Flander, Trappers Lake: Journal of Geophysical Research: Solid Earth, v. 96, no. B8, p. 13,609–13,627, https://doi.org/10.1029/91JB00598.

Gilmer, A.K., Kyle, J.R., Connelly, J.N., Mathur, R.D., and Henry, C.D., 2003, Extension of Laramide magmatism in southwestern North America into Trans-Pecos Texas: Geology, v. 31, no. 5, p. 447–450, https://doi.org/10.1130/0091-7613(2003)031<0447:EOLMIS>2.0.CO;2.

Glazner, A.F., 2022, Cenozoic magmatism and plate tectonics in western North America: Have we got it wrong?, *in* Foulger, G.R., Hamilton, L.C., Jurdy, D.M., Stein, C.A., Howard, K.A., and Stein, S., eds., Footsteps of Warren B. Hamilton: New Ideas in Earth Science: Geological Society of America Special Paper 553, p. 95–108, https://doi.org/10.1130/2021.2553(09).

Golos, E.M., and Fischer, K.M., 2022, New insights into lithospheric structure and melting beneath the Colorado Plateau: Geochemistry, Geophysics, Geosystems, v. 23, no. 3, https://doi.org/10.1029/2021GC010252.

González-León, C.M., Solari, L., Valencia-Moreno, M., Heimpel, M.A.R., Sole, J., Becuar, E.G., Santacruz, R.L., and Arvizu, O.P., 2017, Late Cretaceous to early Eocene magmatic evolution of the Laramide arc in the Nacozari quadrangle, northeastern Sonora, Mexico, and its regional implications: Ore Geology Reviews, v. 81, p. 1137–1157, https://doi.org/10.1016/j.oregeorev.2016.07.020.

Gudfinnsson, G.H., and Presnall, D.C., 2005, Continuous gradations among primary carbonatitic, kimberlitic, melilititic, basaltic, picritic, and komatiitic melts in equilibrium with garnet lherzolite at 3–8 GPa: Journal of Petrology, v. 46, no. 8, p. 1645–1659, https://doi.org/10.1093/petrology/egi029.

Hansen, S.M., Dueker, K.G., Stachnik, J.C., Aster, R.C., and Karlstrom, K.E., 2013, A rootless Rockies—Support and lithospheric structure of the Colorado Rocky Mountains inferred from CREST and TA seismic data: Geochemistry, Geophysics, Geosystems, v. 14, no. 8, p. 2670–2695, https://doi.org/10.1002/ggge.20143.

Hill, B.M., and Bickford, M.E., 2001, Paleoproterozoic rocks of central Colorado: Accreted arcs or extended older crust?: Geology, v. 29, no. 11, p. 1015–1018, https://doi.org/10.1130/0091-7613(2001)029<1015:PROCCA>2.0.CO;2.

Hofmann, A.W., 1997, Mantle geochemistry: The message from oceanic magmatism: Nature, v. 385, p. 219–229, https://doi.org/10.1038/385219a0.

Horton, F., 2015, Did phosphorus derived from the weathering of large igneous provinces fertilize the Neoproterozoic ocean?: Geochemistry, Geophysics, Geosystems, v. 16, no. 6, p. 1723–1738, https://doi.org/10.1002/2015GC005792.

Humphreys, E., Hessler, E., Dueker, K., Farmer, G.L., Erslev, E., and Atwater, T., 2003, How Laramide-age hydration of North American lithosphere by the Farallon slab controlled subsequent activity in the western United States: International Geology Review, v. 45, no. 7, p. 575–595, https://doi.org/10.2747/0020-6814.45.7.575.

Humphreys, E.D., Schmandt, B., Bezada, M.J., and Perry-Houts, J., 2015, Recent craton growth by slab stacking beneath Wyoming: Earth and Planetary Science Letters, v. 429, p. 170–180, https://doi.org/10.1016/j.epsl.2015.07.066.

Irvine, T.N., and Baragar, W.R.A., 1971, A guide to the chemical classification of the common volcanic rocks: Canadian Journal of Earth Sciences, v. 8, p. 523–548, https://doi.org/10.1139/e71-055.

Izett, G.A., 1966, Tertiary Extrusive Volcanic Rocks in Middle Park, Grand County, Colo., *in* Geological Survey Research 1966: U.S. Geological Survey Professional Paper 550B, p. 42–47, https://doi.org/10.3133/pp550B.

Izett, G.A., 1968, Geology of the Hot Sulfur Springs Quadrangle, Grand County, Colorado: U.S. Geological Survey Professional Paper 586, 79 p., https://doi.org/10.3133/pp586.

Jacob, K.H., Farmer, G.L., Buchwaldt, R., and Bowring, S.A., 2015, Deep crustal anatexis, magma mixing, and the generation of epizonal plutons in the Southern Rocky Mountains, Colorado: Contributions to Mineralogy and Petrology, v. 169, no. 1, https://doi.org/10.1007/s00410-014-1094-3.

Jones, C.H., Farmer, G.L., Sageman, B., and Zhong, S., 2011, Hydrodynamic mechanism for the Laramide orogeny: Geosphere, v. 7, no. 1, p. 183–201, https://doi.org/10.1130/GES00575.1.

Kelemen, P.B., Hanghøj, K., and Greene, A.R., 2014, One view of the geochemistry of subduction-related magmatic arcs, with an emphasis on primitive andesite and lower crust, *in* Rudnick, R.L., ed., Treatise on Geochemistry, Volume 4: The Crust (2nd ed.): New York, Elsevier, p. 749–806, https://doi.org/10.1016/B978-0-08-095975-7.00323-5.

Kellogg, K.S., 1999, Neogene basins of the northern Rio Grande rift: Partitioning and asymmetry inherited from Laramide and older uplifts: Tectonophysics, v. 305, no. 1–3, p. 141–152, https://doi.org/10.1016/S0040-1951(99)00013-X.

King, R.L., Bebout, G.E., Moriguti, T., and Nakamura, E., 2006, Elemental mixing systematics and Sr-Nd isotope geochemistry of mélange formation: Obstacles to identification of fluid sources to arc volcanics: Earth and Planetary Science Letters, v. 246, no. 3–4, p. 288–304, https://doi.org/10.1016/j.epsl.2006.03.053.

Kinzler, R.J., 1997, Melting of mantle peridotite at pressures approaching the spinel to garnet transition: Application to mid-ocean ridge basalt petrogenesis: Journal of Geophysical Research: Solid Earth, v. 102, no. B1, p. 853–874, https://doi.org/10.1029/96JB00988.

Knox, K.L., 2005, The Never Summer Igneous Complex: Evolution of a Shallow Magmatic System [M.Sc. thesis]: Boulder, Colorado, University of Colorado, 54 p.

Kuiper, K.F., Deino, A., Hilgen, F.J., Krijgsman, W., Renne, P.R., and Wijbrans, J.R., 2008, Synchronizing rock clocks of Earth history: Science, v. 320, no. 5875, p. 500–504, https://doi.org/10.1126/science.1154339.

Kukuła, A., Puziewicz, J., Matusiak-Malek, M., Ntaflos, T., Büchner, J., and Tietz, O., 2015, Depleted subcontinental lithospheric mantle and its tholeiitic melt metasomatism beneath NE termination of the Eger Rift (Europe): The case study of the Steinberg (Upper Lusatia, SE Germany) xenoliths: Mineralogy and Petrology, v. 109, no. 6, p. 761–787, https://doi.org/10.1007/s00710-015-0405-3.

Kurtz, A.C., Derry, L.A., Chadwick, O.A., and Alfano, M.J., 2000, Refractory element mobility in volcanic soils: Geology, v. 28, no. 8, p. 683–686, https://doi.org/10.1130/0091-7613(2000)28<683:REMIVS>2.0.CO;2.

Lafuente, B., Downs, R.T., Yang, H., and Stone, N., 2015, The power of databases: The RRUFF project, *in* Armbruster, T., and Danis, R.M., eds., Highlights in Mineralogical Crystallography: Berlin, De Gruyter, p. 1–30, https://doi.org/10.1515/9783110417104-003.

Landman, R.L., and Flowers, R.M., 2013, (U-Th)/He thermochronologic constraints on the evolution of the northern Rio Grande rift, Gore Range, Colorado, and implications for rift propagation models: Geosphere, v. 9, no. 1, p. 170–187, https://doi.org/10.1130/GES00826.1.

Larson, E.E., and Drexler, J.W., 1988, Early Laramide mafic to intermediate volcanism, Front Range, Colorado: Colorado School of Mines Quarterly, v. 83, no. 2, p. 41–52.

Larson, E.E., Ozima, M., and Bradley, W.C., 1975, Late Cenozoic basic volcanism in northwestern Colorado and its implications concerning tectonism and the origin of the Colorado River system, *in* Curtis, B.F., ed., Cenozoic History of the Southern Rocky Mountains: Geological Society of America Memoir 144, p. 155–178, https://doi.org/10.1130/MEM144-p155.

Lawton, T.F., and McMillan, N.J., 1999, Arc abandonment as a cause for passive continental rifting: Comparison of the Jurassic Mexican Borderland rift and the Cenozoic Rio Grande rift: Geology, v. 27, no. 9, p. 779–782, https://doi.org/10.1130/0091-7613(1999)027<0779:AAAACF>2.3.CO;2.

Leat, P.T., Thompson, R.N., Morrison, M.A., Hendry, G.L., and Dickin, A.P., 1988a, Compositionally-diverse Miocene-Recent rift-related magmatism in northwest Colorado: Partial melting, and mixing of mafic magmas from 3 different asthenospheric and lithospheric mantle sources: Journal of Petrology, v. 1, p. 351–377, https://doi.org/10.1093/petrology/Special_Volume.1.351.

Leat, P.T., Thompson, R.N., Morrison, M.A., Hendry, G.L., and Dickin, A.P., 1988b, Silicic magmas derived by fractional crystallization from Miocene minette, Elkhead Mountains, Colorado: Mineralogical Magazine, v. 52, no. 368, p. 577–585, https://doi.org/10.1180/minmag.1988.052.368.03.

Leat, P.T., Thompson, R.N., Dickin, A.P., Morrison, M.A., and Hendry, G.L., 1989, Quaternary volcanism in northwestern Colorado—Implications for the roles of asthenosphere and lithosphere in the genesis of continental basalts: Journal of Volcanology and Geothermal Research, v. 37, no. 3–4, p. 291–310, https://doi.org/10.1016/0377-0273(89)90085-1.

Leat, P.T., Thompson, R.N., Morrison, M.A., Hendry, G.L., and Dickin, A.P., 1990, Geochemistry of mafic lavas in the early Rio Grande rift, Yarmony Mountain, Colorado, USA: Chemical Geology, v. 81, no. 1–2, p. 23–43, https://doi.org/10.1016/0009-2541(90)90037-8.

Leat, P.T., Thompson, R.N., Morrison, M.A., Hendry, G.L., and Dickin, A.P., 1991, Alkaline hybrid mafic magmas of the Yampa area, NW Colorado, and their relationship to the Yellowstone mantle plume and lithospheric mantle domains: Contributions to Mineralogy and Petrology, v. 107, no. 3, p. 310–327, https://doi.org/10.1007/BF00325101.

Lee, C.-T.A., Luffi, P., Plank, T., Dalton, H., and Leeman, W.P., 2009, Constraints on the depths and temperatures of basaltic magma generation on Earth and other terrestrial planets using new thermobarometers for mafic magmas: Earth and Planetary Science Letters, v. 279, no. 1–2, p. 20–33, https://doi.org/10.1016/j.epsl.2008.12.020.

Lee, J.Y., Marti, K., Severinghaus, J.P., Kawamura, K., Yoo, H.S., Lee, J.B., and Kim, J.S., 2006, A redetermination of the isotopic abundances of atmospheric Ar: Geochimica et Cosmochimica Acta, v. 70, no. 17, p. 4507–4512, https://doi.org/10.1016/j.gca.2006.06.1563.

Leeman, W.P., and Rogers, J.J.W., 1970, Late Cenozoic alkali-olivine basalts of Basin-Range Province, USA: Contributions to Mineralogy and Petrology, v. 25, no. 1, p. 1–24, https://doi.org/10.1007/BF00383059.

Le Maitre, R.W., ed., 1989, A Classification of Igneous Rocks and Glossary of Terms: Oxford, UK, Blackwell Scientific Publications, 193 p.

Lester, A.P., Larson, E.E., Farmer, G.L., Stern, C.R., and Funk, J.A., 2001, Neoproterozoic kimberlite emplacement in the Front Range, Colorado: Rocky Mountain Geology, v. 36, p. 1–12, https://doi.org/10.2113/gsrocky.36.1.1.

Lin, A.B., Zheng, J.P., Aulbach, S., Xiong, Q., Pan, S.K., and Gerdes, A., 2020, Causes and consequences of wehrlitization beneath a trans-lithospheric fault: Evidence from Mesozoic basalt-borne wehrlite xenoliths from the Tan-Lu fault belt, North China craton: Journal of Geophysical Research: Solid Earth, v. 125, no. 7, https://doi.org/10.1029/2019JB019084.

Lindsay, C.R., and Feeley, T.C., 2003, Magmagenesis at the Eocene Electric Peak–Sepulcher Mountain complex, Absaroka volcanic province, USA: Lithos, v. 67, no. 1–2, p. 53–76, https://doi.org/10.1016/S0024-4937(02)00252-9.

Lipman, P.W., 1980, Cenozoic volcanism in the western United States: Implications for continental tectonics, *in* Burchfiel, B.C., Oliver, J.E., and Silver, L.T., eds., Continental Tectonics: Washington, D.C., National Academy of Sciences, Studies in Geophysics, p. 161–174.

Lipman, P.W., 2007, Incremental assembly and prolonged consolidation of Cordilleran magma chambers: Evidence from the Southern Rocky Mountain volcanic field: Geosphere, v. 3, no. 1, p. 42–70, https://doi.org/10.1130/GES00061.1.

Lipman, P.W., and Glazner, A.F., 1991, Introduction to Middle Tertiary Cordilleran volcanism—Magma sources and relations to regional tectonics: Journal of Geophysical Research: Solid Earth and Planets, v. 96, no. B8, p. 13,193–13,199, https://doi.org/10.1029/91JB01397.

Liu, Y.D., and Ying, J.F., 2020, Origin of clinopyroxene megacrysts in volcanic rocks from the North China craton: A comparison study with megacrysts worldwide: International Geology Review, v. 62, no. 15, p. 1845–1861, https://doi.org/10.1080/00206814.2019.1663766.

Livaccari, R.F., Burke, K., and engör, A.M.C., 1981, Was the Laramide orogeny related to subduction of an oceanic plateau: Nature, v. 289, no. 5795, p. 276–278, https://doi.org/10.1038/289276a0.

Loges, A., Schultze, D., Klugel, A., and Lucassen, F., 2019, Phonolitic melt production by carbonatite mantle metasomatism: Evidence from Eger graben xenoliths: Contributions to Mineralogy and Petrology, v. 174, no. 11, https://doi.org/10.1007/s00410-019-1630-2.

Luedke, R.G., and Smith, R.L., 1978, Map Showing Distribution, Composition, and Age of Late Cenozoic Volcanic Centers in Colorado, Utah, and Southwestern Wyoming: U.S. Geological Survey Miscellaneous Geologic Investigations Map I-1091-B, https://doi.org/10.3133/i1091B.

McCulloch, M.T., and Gamble, J.A., 1991, Geochemical and geodynamical constraints on subduction zone magmatism: Earth and Planetary Science Letters, v. 102, p. 358-374.

McDonough, W.F., and Sun, S.S., 1995, The composition of the Earth: Chemical Geology, v. 120, no. 3–4, p. 223-253.

McKenzie, D., and Bickle, M.J., 1988, The volume and composition of melt generated by extension of the lithosphere: Journal of Petrology, v. 29, p. 625–679, https://doi.org/10.1093/petrology/29.3.625.

Melton, G.L., 2007, Geochemical Characterization of Mantle Xenoliths and the Herring Park Basalt and Their Association to the Rio Grande Rift [M.Sc. thesis]: Golden, Colorado, Colorado School of Mines, 97 p.

Menzies, M., Xu, Y.G., Zhang, H.F., and Fan, W.M., 2007, Integration of geology, geophysics and geochemistry: A key to understanding the North China craton: Lithos, v. 96, no. 1–2, p. 1–21, https://doi.org/10.1016/j.lithos.2006.09.008.

Menzies, M.A., Leeman, W.P., and Hawkesworth, C.J., 1983, Isotope geochemistry of Cenozoic volcanic-rocks reveals mantle heterogeneity below western USA: Nature, v. 303, no. 5914, p. 205–209, https://doi.org/10.1038/303205a0.

Mercer, C.M., Cosca, M.A., and Morgan, L.E., 2024, Argon Data for Samples from the Elkhead and Rabbit Ears Mountains, Northern Colorado, USA: U.S. Geological Survey Data Release, https://doi.org/10.5066/P1VOZBNL.

Millikin, A.E.G., Morgan, L.E., and Noblett, J., 2018, $^{40}Ar/^{39}Ar$ geochronology and petrogenesis of the Table Mountain shoshonite, Golden, Colorado, U.S.A.: Rocky Mountain Geology, v. 53, p. 1–28, https://doi.org/10.24872/rmgjournal.53.1.1.

Min, K.W., Mundil, R., Renne, P.R., and Ludwig, K.R., 2000, A test for systematic errors in Ar-40/Ar-39 geochronology through comparison with U/Pb analysis of a 1.1-Ga rhyolite: Geochimica et Cosmochimica Acta, v. 64, no. 1, p. 73–98, https://doi.org/10.1016/S0016-7037(99)00204-5.

Mirnejad, H., and Bell, K., 2006, Origin and source evolution of the Leucite Hills lamproites: Evidence from Sr-Nd-Pb-O isotopic compositions: Journal of Petrology, v. 47, no. 12, p. 2463–2489, https://doi.org/10.1093/petrology/egl051.

Morozova, E.A., Wan, X., Chamberlain, K.R., Smithson, S.B., Johnson, R., and Karlstrom, K.E., 2005, Inter-wedging nature of the Cheyenne Belt—Archean–Proterozoic suture defined by seismic reflection data, *in* Kalstrom, K.E., and Keller, G.R., eds., The Rocky Mountain Region: An Evolving Lithosphere: American Geophysical Union Geophysical Monograph 154, p. 217–226, https://doi.org/10.1029/154GM15.

Musselman, T.E., 1987, A Modified Crustal Source for the Colorado Mineral Belt: Implications for REE Buffering in CO_2-Rich Fluids [M.Sc. thesis]: Golden, Colorado, Colorado School of Mines, 127 p.

Mutschler, F.E., Larson, E.E., and Bruce, R.M., 1987, Laramide and younger magmatism in Colorado—New petrologic and tectonic variations on old themes: Colorado School of Mines Quarterly, v. 82, no. 4, p. 1–47.

Niu, Y.L., 2021, Lithosphere thickness controls the extent of mantle melting, depth of melt extraction and basalt compositions in all tectonic settings on Earth—A review and new perspectives: Earth-Science Reviews, v. 217, https://doi.org/10.1016/j.earscirev.2021.103614.

Peters, B.J., Day, J.M.D., and Taylor, L.A., 2016, Early mantle heterogeneities in the Reunion hotspot source inferred from highly siderophile elements in cumulate xenoliths: Earth and Planetary Science Letters, v. 448, p. 150–160, https://doi.org/10.1016/j.epsl.2016.05.015.

Pin, C., Briot, D., Bassin, C., and Poitrasson, F., 1994, Concomitant separation of strontium and samarium neodymium for isotopic analysis in silicate samples, based on specific extraction chromatography: Analytica Chimica Acta, v. 298, no. 2, p. 209–217, https://doi.org/10.1016/0003-2670(94)00274-6.

Pivarunas, A.F., and Meert, J.G., 2019, Protracted magmatism and magnetization around the McClure Mountain alkaline igneous complex: Lithosphere, v. 11, no. 5, p. 590–602, https://doi.org/10.1130/L1062.1.

Plank, T., and Forsyth, D.W., 2016, Thermal structure and melting conditions in the mantle beneath the Basin and Range Province from seismology and petrology: Geochemistry, Geophysics, Geosystems, v. 17, no. 4, p. 1312–1338, https://doi.org/10.1002/2015GC006205.

Prothero, D.R., 2011, Magnetobiostratigraphy of the Miocene Troublesome Formation, Middle Park Basin, central Colorado, *in* Sullivan, R.M., Lucas, S.G., and Spielmann, J.A., eds., Fossil Record 3: New Mexico Museum of Natural History and Science Bulletin 53.

Putirka, K., and Platt, B., 2012, Basin and Range volcanism as a passive response to extensional tectonics: Geosphere, v. 8, no. 6, p. 1274–1285, https://doi.org/10.1130/GES00803.1.

Renne, P.R., Mundil, R., Min, K., and Ludwig, K.R., 2005, Intercalibration of the U-Pb and Ar-40/Ar-39 geochronometers: Status, prognosis, and proscription: Geochimica et Cosmochimica Acta, v. 69, no. 10, p. A321–A321.

Righter, K., and Carmichael, I.S.E., 1993, Mega-xenocrysts in alkali olivine basalts—Fragments of disrupted mantle assemblages: The American Mineralogist, v. 78, no. 11–12, p. 1230–1245.

Rosenthal, A., Foley, S.F., Pearson, D.G., Nowell, G.M., and Tappe, S., 2009, Petrogenesis of strongly alkaline primitive volcanic rocks at the propagating tip of the western branch of the East African rift: Earth and Planetary Science Letters, v. 284, no. 1–2, p. 236–248, https://doi.org/10.1016/j.epsl.2009.04.036.

Rosera, J.M., Gaynor, S.P., Ulianov, A., and Schaltegger, U., 2024, Using stochastic point pattern analysis to track regional orientations of magmatism during the transition to Cenozoic extension and Rio Grande rifting, Southern Rocky Mountains: Tectonics, v. 43, no. 2, https://doi.org/10.1029/2023TC007902.

Rowe, M.C., Peate, D.W., and Newbrough, A., 2011, Compositional and thermal evolution of olivine-hosted melt inclusions in small-volume basaltic eruptions: A "simple" example from Dotsero Volcano, NW Colorado: Contributions to Mineralogy and Petrology, v. 161, no. 2, p. 197–211, https://doi.org/10.1007/s00410-010-0526-y.

Sarafian, E., Gaetani, G.A., Hauri, E.H., and Sarafian, A.R., 2017, Experimental constraints on the damp peridotite solidus and oceanic mantle potential temperature: Science, v. 355, no. 6328, p. 942–945, https://doi.org/10.1126/science.aaj2165.

Schwartz, J.J., Lackey, J.S., Miranda, E.A., Klepeis, K.A., Mora-Klepeis, G., Robles, F., and Bixler, J.D., 2023, Magmatic surge requires two-stage model for the Laramide orogeny: Nature Communications, v. 14, no. 1, https://doi.org/10.1038/s41467-023-39473-7.

Shroba, R.R., 2016, Geologic Framework, Age, and Lithologic Characteristics of the North Park Formation in North Park, North-Central Colorado: U.S. Geological Survey Scientific Investigations Report 2016-5126, 28 p., https://doi.org/10.3133/sir20165126.

Shroba, R.R., Bryant, B., Kellogg, K.S., Theobald, P.K., and Brandt, T.R., 2010, Geologic Map of the Fraser 7.5-Minute Quadrangle, Grand County, Colorado: U.S. Geological Survey Scientific Investigations Map 3130, 1 sheet, 26 p. pamphlet, scale 1:24,000, https://pubs.usgs.gov/sim/3130/.

Stein, H.J., and Crock, J.G., 1990, Late Cretaceous–Tertiary magmatism in the Colorado Mineral Belt: Rare earth element and samarium-neodymium isotopic studies, *in* Anderson, J.L., ed., The Nature and Origin of Cordilleran Magmatism: Geological Society of America Memoir 174, p. 195–224, https://doi.org/10.1130/MEM174-p195.

Stoenner, R.W., Schaeffer, O.A., and Katcoff, S., 1965, Half-lives of argon-37, argon-39, and argon-42: Science, v. 148, no. 3675, p. 1325–1328, https://doi.org/10.1126/science.148.3675.1325.

Sun, S.S., and McDonough, W.F., 1989, Chemical and isotopic systematics of oceanic basalts: Implications for mantle composition and processes, *in* Saunders, A.D., and Norry, M.J., eds., Magmatism in the Ocean Basins: Geological Society, London, Special Publication 43, p. 313–345, https://doi.org/10.1144/GSL.SP.1989.042.01.19.

Taylor, R.B., 1975, Geologic Map of the Bottle Pass Quadrangle, Grand County, Colorado: U.S. Geological Survey Geologic Quadrangle 1224, scale 1:24,000, https://doi.org/10.3133/gq1224.

Thompson, R.N., Leat, P.T., Dickin, A.P., Morrison, M.A., Hendry, G.L., and Gibson, S.A., 1990, Strongly potassic mafic magmas from lithospheric mantle sources during continental extension and heating—Evidence from Miocene minettes of northwest Colorado, USA: Earth and Planetary Science Letters, v. 98, no. 2, p. 139–153, https://doi.org/10.1016/0012-821X(90)90055-3.

Thompson, R.N., Gibson, S.A., Leat, P.T., Mitchell, J.G., Morrison, M.A., Hendry, G.L., and Dickin, A.P., 1993, Early Miocene continental extension-related basaltic magmatism at Walton Peak, Northwest Colorado—Further evidence on continental basalt genesis: Journal of the Geological Society, v. 150, p. 277–292, https://doi.org/10.1144/gsjgs.150.2.0277.

Thompson, R.N., Velde, D., Leat, P.T., Morrison, M.A., Mitchell, J.G., Dickin, A.P., and Gibson, S.A., 1997, Oligocene lamproite containing an Al-poor, Ti-rich biotite, Middle Park, northwest Colorado, USA: Mineralogical Magazine, v. 61, no. 407, p. 557–572, https://doi.org/10.1180/minmag.1997.061.407.08.

Tweto, O., 1975, Laramide (Late Cretaceous–early Tertiary) orogeny in the Southern Rocky Mountains, *in* Curtis, B.F., ed., Cenozoic History of the Southern Rocky Mountains: Geological Society of America Memoir 144, p. 1–44, https://doi.org/10.1130/MEM144-p1.

Tweto, O., 1979, The Rio Grande rift in Colorado, *in* Rieker, R.E., ed., Rio Grande Rift: Tectonics and Magmatism: Washington, D.C., American Geophysical Union, p. 33–56.

Valencia-Moreno, M., Camprubí, A., Ochoa-Landín, L., Calmus, T., and Mendívil-Quijada, H., 2017, Latest Cretaceous–early Paleogene "boom" of porphyry Cu mineralization associated with the Laramide magmatic arc of Mexico: Ore Geology Reviews, v. 81, p. 1113–1124, https://doi.org/10.1016/j.oregeorev.2016.05.005.

van Wijk, J.W., Baldridge, W.S., Van Hunen, J., Goes, S., Aster, R., Coblentz, D.D., Grand, S.P., and Ni, J., 2010, Small-scale convection at the edge of the Colorado Plateau: Implications for topography, magmatism, and evolution of Proterozoic lithosphere: Geology, v. 38, no. 7, p. 611–614, https://doi.org/10.1130/G31031.1.

Walter, M.J., 1998, Melting of garnet peridotite and the origin of komatiite and depleted lithosphere: Journal of Petrology, v. 39, p. 29–60, https://doi.org/10.1093/petroj/39.1.29.

Wannamaker, P.E., Hasterok, D.P., Johnston, J.M., Stodt, J.A., Hall, D.B., Sodergren, T.L., Pellerin, L., Maris, V., Doerner, W.M., Groenewold, K.A., and Unsworth, M.J., 2008, Lithospheric dismemberment and magmatic processes of the Great Basin–Colorado Plateau transition, Utah, implied from magnetotellurics: Geochemistry, Geophysics, Geosystems, v. 9, Q05019, https://doi.org/10.1029/2007GC001886.

Weidendorfer, D., Manning, C.E., and Schmidt, M.W., 2020, Carbonate melts in the hydrous upper mantle: Contributions to Mineralogy and Petrology, v. 175, no. 8, https://doi.org/10.1007/s00410-020-01708-x.

Whitmeyer, S.J., and Karlstrom, K.E., 2007, Tectonic model for the Proterozoic growth of North America: Geosphere, v. 3, no. 4, p. 220–259, https://doi.org/10.1130/GES00055.1.

Wilson, M.D., 2002, Petrographic provenance analysis of Kiowa Core sandstone samples, Denver Basin, CO: Rocky Mountain Geology, v. 37, p. 173–187, https://doi.org/10.2113/6.

Wood, B.J., Kiseeva, E.S., and Matzen, A.K., 2013, Garnet in the Earth's mantle: Elements, v. 9, no. 6, p. 421–426, https://doi.org/10.2113/gselements.9.6.421.

Wrucke, W.T., 1974, The Whitehorn Granodiorite of the Arkansas Valley in Central Colorado: U.S. Geological Survey Bulletin 1394, 16 p., https://pubs.usgs.gov/bul/1394h/report.pdf.

Wu, F.Y., Yang, J.H., Xu, Y.G., Wilde, S.A., and Walker, R.J., 2019, Destruction of the North China craton in the Mesozoic: Annual Review of Earth and Planetary Sciences, v. 47, p. 173–195, https://doi.org/10.1146/annurev-earth-053018-060342.

Xia, L.Q., Li, X.M., Ma, Z.P., Xu, X.Y., and Xia, Z.C., 2011, Cenozoic volcanism and tectonic evolution of the Tibetan Plateau: Gondwana Research, v. 19, no. 4, p. 850–866, https://doi.org/10.1016/j.gr.2010.09.005.